Electronic Supplementary Information

Tuning the Interlocking in Partially Saturated Copper(I) Rotaxane Complexes for O_2-to-H_2O Electrocatalytic Reduction

Yan Zhang,[†a] Hei Tung Yau,[†ab] Qi-Fa Chen,[ac] Yulin Deng,[ac] Zhuoliang Ying,[a] Seungkyu Lee,*[a] Ho Yu Au-Yeung*[ac] and Edmund C. M. Tse*[abd]

[a] Department of Chemistry, The University of Hong Kong, Hong Kong SAR, China

[b] HKU-CAS Joint Laboratory on New Materials, The University of Hong Kong, Hong Kong SAR, China

[c] State Key Laboratory of Synthetic Chemistry, The University of Hong Kong, Hong Kong SAR, China

[d] HKU Shenzhen Institute of Research and Innovation (HKU-SIRI), Shenzhen 518057, China

[†] These authors contributed equally: Hei Tung Yau and Yan Zhang

[*] Corresponding authors: SL (skchem@hku.hk); HYA (hoyuay@hku.hk); ECMT (ecmtse@hku.hk)

List of Contents

1. Molecular Syntheses and Characterisations.

1.1 Syntheses.

General. All reagents (purity ≥98% unless otherwise noted) were purchased from commercial suppliers (J&K, Sigma-Aldrich, TCI, Aladdin, Energy, Macklin, and Dkmchem) and used without further purification unless otherwise noted. All the solvents were of analytical grade (ACI Labscan and DUKSAN Pure Chemicals). Deuterated solvents $CDCl_3$ and CD_3CN were purchased from Cambridge Isotope Laboratories (CIL) (≥99.8 atom% D). Compounds **1**, **3**, **5**, **M4**, **M6**, **M8**, and **M10** were synthesized according to literature procedures.[1-3] Thin layer chromatography (TLC) was performed on silica gel 60 F254 (Merck, Germany, Aluminium sheet) and column chromatography was carried out using silica gel F60 (Silicycle, Canada). HR-ESI-MS were obtained from a Bruker Impact II Ultra-High Resolution QTOF mass spectrometer. NMR spectra were recorded on Bruker DPX spectrometers with working frequencies at 400 MHz, 500 MHz, or 600 MHz for ^1H, and 101 MHz, 126 MHz, or 151 MHz for ^{13}C, respectively. Chemical shifts were reported in ppm and referenced to solvent residues (for ^1H: $CDCl_3$: δ = 7.26 ppm, CD_3CN: δ = 1.94 ppm; for ^{13}C: $CDCl_3$: δ = 77.16 ppm, CD_3CN: δ = 1.32 ppm and 118.26 ppm).

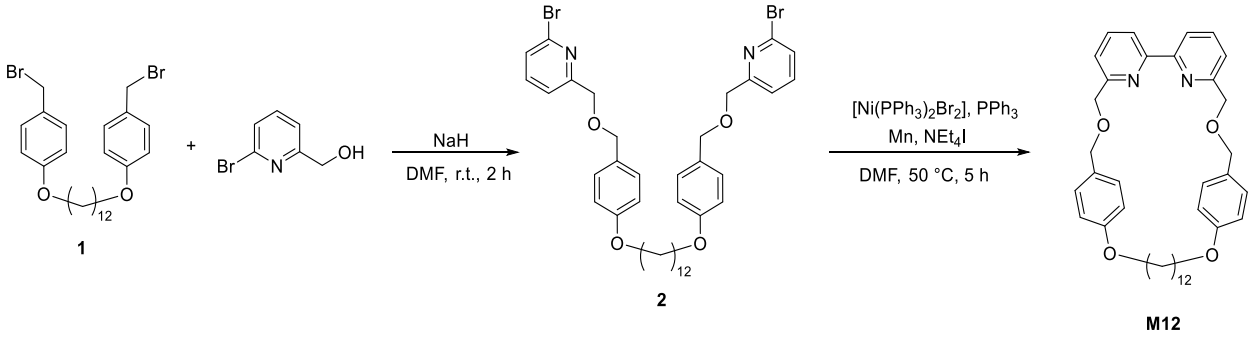

Scheme S1. Synthesis of **M12**.

*Synthesis of **2***. To a solution of 2-bromo-6-pyridinemethanol (432 mg, 0.8 mmol) in 10 mL of dimethylformamide (DMF) at 0 °C was added 60 wt% NaH (64 mg, 1.6 mmol) in three portions with continuous stirring. After stirring at 0 °C for 30 minutes, compound **1** (358 mg, 0.7 mmol) was added and the mixture was stirred at 0 °C for 1 hour. The reaction mixture was warmed up to room temperature, and water was added (10 mL) dropwise. The solvents were removed using a rotary evaporator, and the residue was redissolved in CH_2Cl_2 (50 mL), washed with water (2 × 10 mL) and brine (10 mL), dried over Na_2SO_4 and filtered. Solvents were removed from the filtrate using a rotary evaporator to afford a yellow oil, which was purified using a silica column (eluent:

CH_2Cl_2/hexane, *v*/*v* = 1:1) to give **2** as a white solid. Yield = 0.49 g, 65%. ^{1}H NMR (500 MHz, $CDCl_3$, 298 K) δ 7.55 (t, *J* = 8.0 Hz, 2H), 7.46 (d, *J* = 7.5 Hz, 2H), 7.37 (d, *J* = 8.0 Hz, 2H), 7.28 (d, *J* = 8.5 Hz, 4H), 6.88 (d, *J* = 8.5 Hz, 4H), 4.62 (s, 4H), 4.56 (s, 4H), 3.95 (t, *J* = 7.0 Hz, 4H), 1.77 (p, *J* = 7.0 Hz, 4H), 1.45 (p, *J* = 7.8 Hz, 4H), 1.36–1.23 (m,12H). ^{13}C{^{1}H} NMR (126 MHz, $CDCl_3$, 298 K) δ 159.0, 141.4, 139.1, 129.7, 126.7, 120.1, 114.6, 73.0, 72.1, 68.2, 29.7, 29.5, 29.4, 26.2. HRMS (ESI+): *m/z* calcd. for $C_{38}H_{47}N_2O_4Br_2$ $[M+H]^+$: 755.1881, found: 755.1879.

*Synthesis of **M12***. Under an argon atmosphere, a mixture of $[Ni(PPh_3)_2Br_2]$ (1.49 g, 2.0 mmol), PPh_3 (1.05 g, 4.0 mmol), manganese powder (1.10 g, 20.0 mmol) and NEt_4I (0.51 g, 2.0 mmol) in DMF (20 mL) was sonicated for 10 minutes, and the mixture was heated at 50 °C for 1 hour. To this mixture was slowly added a solution of compound **2** (1.51 g, 2.0 mmol) in DMF (20 mL) over 4 hours, and the reaction mixture was heated at 50 °C for another 1 hour. The reaction mixture was cooled to room temperature, CH_2Cl_2 (50 mL) and a saturated solution of Na_2EDTA in aqueous ammonia (17.5 wt%, 50 mL) were added, the mixture was then filtered through a Celite pad. The filtrate was washed with water (2 × 50 mL) and brine (50 mL), dried over Na_2SO_4, and the solvents were removed using a rotary evaporator. The crude product was purified by a silica column with a gradient elution with an increasing amount of CH_3CN from 0% to 10% in CH_2Cl_2/hexane (*v*/*v* 1:1). Macrocycle **M12** was obtained as a white solid. Yield = 0.27 g, 54%. ^{1}H NMR (500 MHz, CD_3CN, 298 K) δ 8.14 (d, *J* = 7.5 Hz, 2H), 7.81 (t, *J* = 8.0 Hz, 2H), 7.40 (d, *J* = 7.5 Hz, 2H), 7.22 (d, *J* = 8.5 Hz, 4H), 6.79 (d, *J* = 8.5 Hz, 4H), 4.63 (s, 4H), 4.58 (s, 4H), 3.93 (t, *J* = 6.5 Hz, 4H), 1.65 (p, *J* = 7.0 Hz, 4H), 1.37 (p, *J* = 8.0 Hz, 4H), 1.27–1.19 (m, 12H). ^{13}C{^{1}H} NMR (126 MHz, CD_3CN, 298 K) δ 159.6, 159.3, 156.3, 138.4, 131.4, 130.8, 123.1, 120.4, 115.3, 73.4, 73.0, 68.4, 30.1, 29.9, 29.5, 29.4, 26.3. HRMS (ESI+): *m/z* calcd. for $C_{38}H_{47}N_2O_4$ $[M+H]^+$: 595.3530, found: 595.3520.

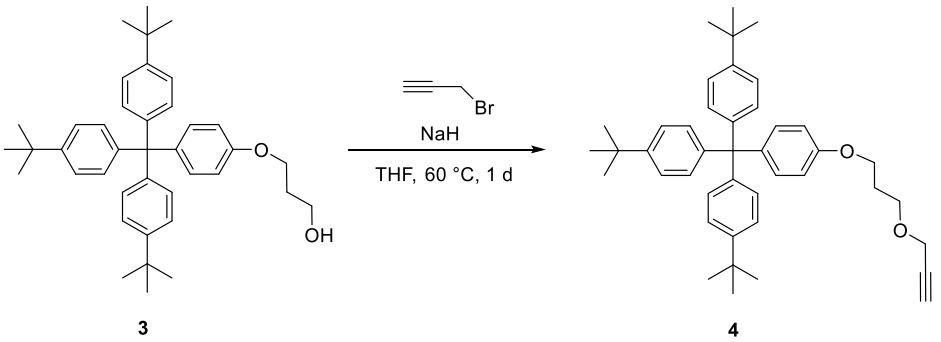

Scheme S2. Synthesis of **4**.

*Synthesis of **4***. To a solution of compound **3** (456 mg, 0.8 mmol) in THF (10 mL) at 0 °C was added 60 wt% NaH (64 mg, 1.6 mmol) in three portions with continuous stirring. After stirring at 0 °C for 30 minutes, propargyl bromide (0.1 mL, 0.96 mmol) was added, the solution was stirred at 0 °C for 1 hour. The reaction mixture was warmed to room temperature, and subsequently quenched by adding water (10 mL) dropwise. Solvents were removed using a rotary evaporator and the residue was redissolved in CH_2Cl_2 (50 mL), washed with water (2 × 10 mL) and brine (10 mL). The organic layer was dried over Na_2SO_4, filtered, solvents of the filtrate was removed using a rotary evaporator to afford a yellow oil residue, which was purified using a silica column (eluent: CH_2Cl_2/hexane, *v*/*v* = 1:5) to afford **4** as a pale yellow solid. Yield = 0.35 g, 73%. ^{1}H NMR (500 MHz, $CDCl_3$, 298 K) δ 7.23 (d, *J* = 8.5 Hz, 6H), 7.09–7.07 (m, 8H), 6.77 (d, *J* = 8.5 Hz, 2H), 4.15 (d, *J* = 2.5 Hz, 2H), 4.04 (t, *J* = 6.5 Hz, 2H), 3.70 (t, *J* = 6.0 Hz, 2H), 2.39 (t, *J* = 2.5 Hz, 1H), 2.06 (p, *J* = 6.0 Hz, 2H), 1.30 (s, 27H). ^{13}C{^{1}H} NMR (126 MHz, $CDCl_3$, 298 K) δ 156.8, 148.4, 144.3, 139.7, 132.4, 130.8, 124.2, 113.2, 80.0, 74.4, 66.9, 64.7, 63.2, 58.4, 34.4, 31.5, 29.8. HRMS (ESI+): *m/z* calcd. for $C_{43}H_{53}O_2$ $[M+H]^+$: 601.4040, found: 601.4043.

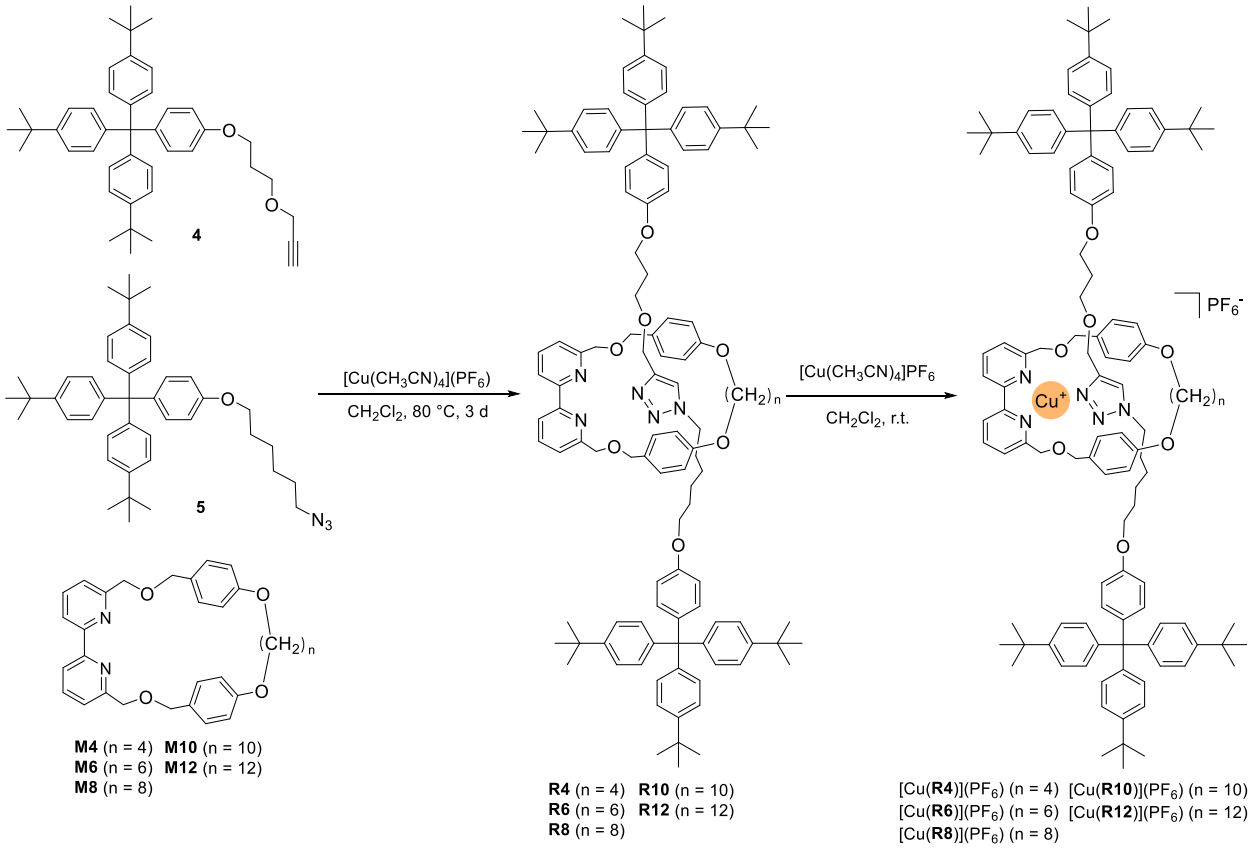

Scheme S3. Active template synthesis of the rotaxane ligands and Cu^{I} complexes.

General procedures for the synthesis of [2]rotaxane ligands and the Cu^{I} complexes. Under an argon atmosphere, a mixture of the macrocycle (25 μmol) and $[Cu(MeCN)_4](PF_6)$ (9.3 mg, 25 μmol) in CH_2Cl_2 (1 mL) was stirred at room temperature for 30 minutes to give an orange colour solution, and then a mixture of **3** (45.1 mg, 75 μmol) and **5** (47.2 mg, 75 μmol) in CH_2Cl_2 (1.5 mL) was added and heated at 80 °C for 3 days. The reaction mixture was cooled to room temperature, diluted with CH_2Cl_2 (50 mL), and washed with a saturated solution of Na_2EDTA in aqueous ammonia (17.5 wt%, 50 mL). The organic layer was collected and the aqueous phase was extracted with CH_2Cl_2 (3 × 10 mL). The organic phases were combined and dried over Na_2SO_4, filtered, and solvents from the filtrate were removed using a rotary evaporator. The crude product was purified using a silica column (gradient elution: from *v*/*v* = 1:1 CH_2Cl_2/hexane to *v*/*v*/v = 2:2:1 CH_2Cl_2/hexane/MeCN) to give the [2]rotaxanes.

To obtain the Cu^{I} complexes, an equimolar mixture of the rotaxane ligand (10 μmol) and $[Cu(MeCN)_4](PF_6)$ (10 μmol) in CH_2Cl_2 (10 mL) was stirred at room temperature for 1 hour under

an argon atmosphere. The reaction mixture was then filtered through a Celite pad, and solvents in the filtrate were removed using a rotary evaporator to give the Cu^{I} rotaxane complexes (as hexafluorophosphate salts) as a red solid.

R4: White solid, yield = 31 mg, 74%. ^{1}H NMR (600 MHz, *v*/*v* = 1:2 $CDCl_3$/CD_3CN, 298 K) δ 7.74 (s, 1H), 7.62 (t, *J* = 7.8 Hz, 2H), 7.46 (d, *J* = 7.8, 2H), 7.35 (d, *J* = 7.8 Hz, 2H), 7.32–7.25 (m, 12H), 7.16 (d, *J* = 8.4 Hz, 6H), 7.11 (d, *J* = 9.0 Hz, 6H), 7.04 (d, *J* = 9.0 Hz, 2H), 6.99 (d, *J* = 9.0 Hz, 2H), 6.96 (d, *J* = 8.4 Hz, 4H), 6.63–6.60 (m, 8H), 4.47 (d, *J* = 12.0 Hz, 2H), 4.41 (d, *J* = 11.4 Hz, 2H), 4.39 (s, 2H), 4.24 (d, *J* = 12.6 Hz, 2H), 4.21 (d, *J* = 12.6 Hz, 2H), 4.05–4.00 (m, 2H), 3.97–3.92 (m, 2H), 3.81 (t, *J* = 6.6 Hz, 2H), 3.47 (t, *J* = 6.0 Hz, 2H), 3.40 (t, *J* = 6.6 Hz, 2H), 3.37 (t, *J* = 7.8 Hz, 2H), 1.85–1.79 (m, 6H), 1.27 (s, 27H), 1.26 (s, 27H), 1.02 (p, *J* = 7.2 Hz, 2H), 0.75 (p, *J* = 7.8 Hz, 2H), 0.59 (p, *J* = 7.8 Hz, 2H), 0.44 (p, *J* = 7.8 Hz, 2H). ^{13}C{^{1}H} NMR (151 MHz, *v*/*v* = 1:2 $CDCl_3$/CD_3CN, 298 K) δ 159.9, 159.7, 157.8, 157.7, 157.5, 149.4, 145.6, 145.5, 145.0, 140.2, 139.9, 138.2, 132.4, 132.4, 131.3, 131.2, 131.2, 130.7, 130.6, 125.4, 125.4, 124.4, 121.9, 121.9, 115.8, 114.3, 114.2, 73.1, 71.7, 68.1, 67.5, 67.4, 65.7, 65.0, 64.0, 63.9, 50.1, 34.9, 31.5, 30.3, 30.2, 29.8, 29.0, 27.7, 26.2, 25.5, 25.4. IR (cm^{-1}): 2955, 2920, 2859, 1607, 1578, 1506, 1457, 1363, 1248, 1182, 1092, 1018, 821, 704, 626, 579. HRMS (ESI+): *m/z* calcd. for $C_{116}H_{138}N_5O_7$ $[M+H]^+$: 1714.0624, found: 1714.0601.

[Cu(**R4**)](PF_6): Orange solid, yield = 18 mg, 93%. ^{1}H NMR (600 MHz, CD_3CN, 298 K) δ 7.82 (br, 4H), 7.59 (br, 2H), 7.48 (s, 1H), 7.31 (d, *J* = 6.6 Hz, 6H), 7.28 (d, *J* = 8.4 Hz, 6H), 7.19 (d, *J* = 8.4 Hz, 6H), 7.12 (d, *J* = 9.0 Hz, 6H), 7.07 (d, *J* = 9.0 Hz, 2H), 7.03 (d, *J* = 8.4 Hz, 2H), 6.93 (d, *J* = 7.8 Hz, 4H), 6.77–6.74 (m, 6H), 6.31 (d, *J* = 8.4 Hz, 2H), 4.66 (br, 2H), 4.38 (t, *J* = 7.2 Hz, 2H), 4.25–4.13 (m, 6H), 4.07–4.04 (m, 4H), 3.95 (t, *J* = 6.6 Hz, 2H), 3.25 (br, 2H), 3.02 (br, 2H), 2.77 (br, 2H), 2.03–1.95 (m, 6H), 1.78 (p, *J* = 6.6 Hz, 2H), 1.55 (p, *J* = 7.2 Hz, 2H), 1.40 (p, *J* = 3.0 Hz, 2H), 1.26 (d, *J* = 1.8 Hz, 54H), 1.14–1.11 (m, 2H). ^{13}C{^{1}H} NMR (151 MHz, CD_3CN, 298 K) δ 159.8, 157.8, 157.0, 149.4, 149.4, 145.6, 145.5, 140.6, 140.5, 140.3, 132.6, 132.4, 131.1, 130.7, 125.5, 125.4, 116.0, 114.2, 113.8, 72.8, 71.3, 68.4, 67.8, 64.5, 64.0, 63.9, 34.9, 34.9, 31.5, 30.4, 30.3, 29.7, 27.7, 26.8, 26.0, 25.7. IR (cm^{-1}): 2958, 2928, 2864, 1606, 1578, 1505, 1467, 1393, 1363, 1300, 1245, 1174, 1080, 1016, 839, 819, 703, 624, 583, 556. HRMS (ESI+): *m/z* calcd. for $C_{116}H_{137}N_5O_7Cu$ $[M-PF_6]^+$: 1775.9842, found: 1775.9812.

R6: White solid, yield = 31 mg, 71%. ^{1}H NMR (600 MHz, *v*/*v* = 1:2 $CDCl_3$/CD_3CN, 298 K) δ 7.64 (d, *J* = 7.8 Hz, 2H), 7.59 (t, *J* = 7.8 Hz, 2H), 7.55 (s, 1H), 7.37 (d, *J* = 7.8 Hz, 2H), 7.27–7.21 (m, 12H), 7.13 (d, *J* = 9.0 Hz, 6H), 7.09 (d, *J* = 8.4 Hz, 6H), 7.01 (d, *J* = 8.4 Hz, 2H), 6.97–6.93 (m, 6H), 6.55 (d, *J* = 9.0 Hz, 4H), 6.51–6.45 (m, 4H), 4.47 (s, 4H), 4.37 (s, 6H), 3.79 (t, *J* = 6.6 Hz, 4H), 3.74 (t, *J* = 6.6 Hz, 2H), 3.59 (t, *J* = 7.8 Hz, 2H), 3.43 (t, *J* = 6.0 Hz, 2H), 3.38 (t, *J* = 6.6 Hz, 2H), 1.80 (p, *J* = 6.6 Hz, 2H), 1.58 (p, *J* = 6.6 Hz, 4H), 1.31–1.28 (m, 4H), 1.26 (d, *J* = 3.0 Hz, 54H), 1.09 (p, *J* = 6.6 Hz, 2H), 1.04 (p, *J* = 7.8, 2H), 0.71 (p, *J* = 7.2 Hz, 2H), 0.57 (p, *J* = 7.8 Hz, 2H). ^{13}C{^{1}H} NMR (151 MHz, *v*/*v* = 1:2 $CDCl_3$/CD_3CN, 298 K) δ 159.8, 157.8, 157.7, 149.4, 145.6, 145.4, 140.2, 140.1, 138.3, 132.7, 131.5, 130.8, 125.4, 124.1, 121.8, 121.4, 115.6, 114.3, 114.2, 72.9, 71.9, 68.5, 68.2, 67.8, 65.7, 65.2, 64.1, 64.0, 50.5, 35.1, 32.0, 30.5, 29.8, 29.4, 28.0, 26.6, 26.2, 25.8. IR (cm^{-1}): 2951, 2920, 2854, 1644, 1607 1579, 1507, 1459, 1361, 1244, 1181, 1090, 1016, 821, 786, 703, 624, 579. HRMS (ESI+): *m/z* calcd. for $C_{118}H_{142}N_5O_7$ $[M+H]^+$: 1742.0937, found: 1742.0916.

[Cu(**R6**)](PF_6): Orange solid, yield = 18 mg, 92%. ^{1}H NMR (600 MHz, CD_3CN, 298 K) δ 8.04 (d, *J* = 8.4 Hz, 2H), 7.96 (t, *J* = 7.8 Hz, 2H), 7.68 (d, *J* = 7.8 Hz, 2H), 7.29–7.27 (m, 12H), 7.15–7.13 (m, 12H), 7.10 (d, *J* = 9.0 Hz, 2H), 7.07 (d, *J* = 9.0 Hz, 2H), 7.05 (s, 1H), 6.88 (d, *J* = 8.4 Hz, 4H), 6.77 (d, *J* = 9.0 Hz, 2H), 6.64–6.61 (m, 6H), 4.52 (d, *J* = 12.6 Hz, 2H), 4.37 (d, *J* = 12.6 Hz, 2H), 4.34–4.28 (m, 4H), 4.11 (t, *J* = 7.2 Hz, 2H), 3.95–3.90 (m, 6H), 3.72 (t, *J* = 6.0 Hz, 2H), 3.61 (t, *J* = 6.0 Hz, 2H), 3.19 (t, *J* = 6.0 Hz, 2H), 1.77–1.74 (m, 6H), 1.72–1.69 (m, 2H), 1.63 (t, *J* = 6.0 Hz, 2H), 1.57–1.52 (m, 4H), 1.45 (p, *J* = 7.8 Hz, 2H) 1.26 (d, *J* = 2.6 Hz, 54H), 1.24–1.22 (m, 2H). ^{13}C{^{1}H} NMR (151 MHz, CD_3CN, 298 K) δ 159.4, 158.9, 157.8, 157.5, 149.4, 149.4 145.5, 145.2, 140.5, 140.4, 140.2, 132.6, 132.5, 131.1, 130.1, 130.0, 125.4, 124.2, 123.4, 121.4, 115.2, 114.3, 114.2, 72.3, 70.7, 68.4, 68.2, 68.0, 65.0, 64.2, 63.9, 51.5, 34.9, 31.5, 30.4, 30.3, 29.9, 29.8, 29.6, 26.7, 26.3, 26.0. IR (cm^{-1}): 2956, 2927, 2864, 1609, 1576, 1505, 1467, 1394, 1361, 1244, 1173, 1105, 1083, 1016, 839, 821, 791, 705, 624, 583, 556, 528. HRMS (ESI+): *m/z* calcd. for $C_{118}H_{141}N_5O_7Cu$ $[M-PF_6]^+$: 1805.0159, found: 1805.0133.

R8: White solid, yield = 35 mg, 79%. ^{1}H NMR (600 MHz, *v*/*v* = 1:2 $CDCl_3$/CD_3CN, 298 K) δ 7.85 (d, *J* = 7.8 Hz, 2H), 7.56 (t, *J* = 7.8 Hz, 2H), 7.42 (s, 1H), 7.35 (d, *J* = 7.2 Hz, 2H), 7.26–7.23 (m, 12H), 7.13–7.07 (m, 12H), 6.98–6.95 (m, 6H), 6.91 (d, *J* = 9.0 Hz, 2H), 6.54 (d, *J* = 8.4 Hz, 4H), 6.41 (d, *J* = 9.0 Hz, 2H), 6.38 (d, *J* = 9.0 Hz, 2H), 4.50 (s, 4H), 4.47 (s, 4H), 4.40 (s, 2H),

3.82 (t, *J* = 7.8 Hz, 2H), 3.74–3.70 (m, 6H), 3.46 (t, *J* = 6.6 Hz, 2H), 3.38 (t, *J* = 6.0 Hz, 2H), 1.80 (p, *J* = 6.0 Hz, 2H), 1.52 (p, *J* = 6.6 Hz, 4H), 1.33–1.30 (m, 2H), 1.27 (d, *J* = 3.6 Hz, 54H), 1.21–1.16 (m, 6H), 1.09 (p, *J* = 3.6 Hz, 4H), 0.88 (m, *J* = 7.8 Hz, 2H), 0.79 (q, *J* = 8.4 Hz, 2H). $^{13}C\{^{1}H\}$ NMR (151 MHz, *v*/*v* = 1:2 $CDCl_3/CD_3CN$, 298 K) δ 159.6, 157.8, 157.7, 149.3, 145.7, 145.6,140.2, 140.1, 138.3, 132.7, 131.5, 130.9, 130.7, 125.4, 123.9, 122.3, 120.8, 115.4, 114.2, 72.9, 72.5, 68.4, 68.2, 67.9, 65.6, 65.2, 64.1, 64.0, 50.7, 35.2, 32.0, 30.8, 30.5, 30.1, 29.8, 29.6, 26.8, 26.0. IR (cm^{-1}): 2955, 2930, 2862, 1607, 1576, 1503, 1460, 1440, 1393, 1360, 1298, 1242, 1181, 1105, 1087, 1017, 817, 786, 703, 622, 579, 528. HRMS (ESI+): *m/z* calcd. for $C_{120}H_{146}N_5O_7$ $[M+H]^+$: 1770.1250, found: 1770.1212.

[Cu(**R8**)](PF_6): Orange solid, yield = 19 mg, 95%. ^{1}H NMR (600 MHz, CD_3CN, 298 K) δ 8.11 (d, *J* = 7.8 Hz, 2H), 8.00 (t, *J* = 7.8 Hz, 2H), 7.71 (d, *J* = 7.8 Hz, 2H), 7.28–7.25 (m, 12H), 7.14–7.08 (m, 17H), 6.90 (d, *J* = 8.4 Hz, 4H), 6.76 (d, *J* = 9.0 Hz, 2H), 6.71 (d, *J* = 9.0 Hz, 2H), 6.59 (d, *J* = 8.4 Hz, 4H), 4.51–4.37 (m, 8H), 3.97 (t, *J* = 7.2 Hz, 2H), 3.95–3.81 (m, 10H), 3.22 (t, *J* = 6.0 Hz, 2H), 1.75–1.71 (m, 2H), 1.69–1.63 (m, 6H), 1.58 (p, *J* = 7.8 Hz, 2H), 1.50 (q, *J* = 7.8, 6.2 Hz, 4H), 1.40–1.37 (m, 6H), 1.25 (d, *J* = 3.0 Hz, 54H), 1.18–1.14 (m, 2H). $^{13}C\{^{1}H\}$ NMR (151 MHz, CD_3CN, 298 K) δ 159.5, 158.8, 157.8, 157.6, 151.8, 149.4, 145.8, 145.5, 140.5, 140.4, 140.0, 132.6, 131.2, 130.2, 129.8, 125.4, 124.1, 123.9, 121.4, 115.0, 114.3, 72.2, 70.8, 68.3, 68.3, 67.8, 65.3, 64.0, 63.9, 51.4, 34.9, 31.5, 30.3, 30.1, 29.7, 29.7, 29.5, 26.7, 26.7, 26.0. IR (cm^{-1}): 2955, 2902, 2864, 1607, 1576, 1503, 1465, 1393, 1363, 1244, 1174, 1105, 1082, 1016, 839, 819, 703, 622, 583, 555, 525. HRMS (ESI+): *m/z* calcd. for $C_{120}H_{145}N_5O_7Cu$ $[M-PF_6]^+$: 1833.0472, found: 1833.0428.

R10: White solid, yield = 38 mg, 85%. ^{1}H NMR (600 MHz, *v*/*v* = 1:2 $CDCl_3/CD_3CN$, 298 K) δ 7.98 (d, *J* = 7.8 Hz, 2H), 7.55 (t, *J* = 7.8 Hz, 2H), 7.39 (s, 1H), 7.30 (d, *J* = 7.2 Hz, 2H), 7.26–7.23 (m, 12H), 7.11–7.07 (m, 12H), 6.98–6.93 (m, 8H), 6.52 (d, *J* = 8.4 Hz, 4H), 6.46 (d, *J* = 9.0 Hz, 2H), 6.39 (d, *J* = 8.4 Hz, 2H), 4.51 (d, *J* = 4.8 Hz, 8H), 4.41 (s, 2H), 3.94 (t, *J* = 7.8 Hz, 2H), 3.74–3.71 (m, 6H), 3.47 (t, *J* = 6.0 Hz, 2H), 3.41 (t, *J* = 6.0 Hz, 2H), 1.81 (p, *J* = 6.0 Hz, 2H), 1.54 (p, *J* = 6.6 Hz, 4H), 1.45 (p, *J* = 7.8 Hz, 2H), 1.27 (d, *J* = 4.2 Hz, 54H), 1.25–1.20 (m, 6H), 1.13–1.07 (m, 8H), 0.99 (p, *J* = 7.8 Hz, 2H), 0.94–0.90 (m, 2H). $^{13}C\{^{1}H\}$ NMR (151 MHz, *v*/*v* = 1:2 $CDCl_3/CD_3CN$, 298 K) δ 159.6, 159.4, 157.8, 157.7, 156.4, 149.4, 145.7, 140.3, 140.2, 138.4, 132.7, 131.5, 130.8, 125.5, 123.9, 122.8, 120.7, 115.3, 114.2, 73.1, 73.1, 68.6, 68.3, 68.0, 65.7,

65.2, 64.1, 50.8, 35.2, 32.1, 30.9, 30.5, 30.5, 29.9, 29.8, 29.7, 26.9, 26.8, 26.2. IR (cm^{-1}): 2953, 2930, 2863, 1609, 1578, 1506, 1461, 1439, 1393, 1363, 1298, 1244, 1182, 1108, 1077, 1018, 821, 788, 706, 626, 581, 530. HRMS (ESI+): *m/z* calcd. for $C_{122}H_{150}N_5O_7$ $[M+H]^+$: 1798.1563, found: 1798.1538.

[Cu(**R10**)](PF_6): Orange solid, yield = 19 mg, 93%. ^1H NMR (600 MHz, CD_3CN, 298 K) δ 8.12 (d, *J* = 7.8 Hz, 2H), 8.01 (t, *J* = 7.8 Hz, 2H), 7.71 (d, *J* = 7.8 Hz, 2H), 7.37 (s, 1H), 7.30–7.24 (m, 12H), 7.16–7.07 (m, 16H), 6.91 (d, *J* = 8.4 Hz, 4H), 6.75 (d, *J* = 9.0 Hz, 2H), 6.68 (d, *J* = 9.0 Hz, 2H), 6.62 (d, *J* = 9.0 Hz, 4H), 4.51–4.42 (m, 8H), 3.97–3.91 (m, 4H), 3.89–3.81 (m, 6H), 3.79 (t, *J* = 6.0 Hz, 2H), 3.19 (t, *J* = 6.0 Hz, 2H), 1.68 (p, *J* = 7.2, 6.6 Hz, 6H), 1.61–1.51 (m, 4H), 1.45 (p, *J* = 7.2 Hz, 4H), 1.36–1.31 (m, 10H), 1.26 (d, *J* = 1.8 Hz, 54H), 1.09 (q, *J* = 7.8 Hz, 2H). $^{13}C\{^1H\}$ NMR (151 MHz, CD_3CN, 298 K) δ 159.6, 158.8, 157.8, 157.6, 151.8, 149.4, 145.7, 145.5, 145.5, 140.5, 140.4, 140.0, 132.6, 132.6, 131.2, 130.2, 130.0, 125.4, 124.6, 124.2, 121.5, 114.9, 114.3, 72.4, 71.3, 68.5, 68.3, 67.8, 65.4, 63.9, 63.8, 51.3, 34.9, 31.5, 30.3, 30.3, 30.0, 29.7, 29.6, 29.5, 29.4, 26.6, 26.6, 25.9. IR (cm^{-1}): 2956, 2920, 2862, 1647, 1606, 1579, 1497, 1466, 1391, 1362, 1300, 1245, 1175, 1103, 1083, 1019, 840, 822, 703, 625, 579, 554, 528. HRMS (ESI+): *m/z* calcd. for $C_{122}H_{149}N_5O_7Cu$ $[M-PF_6]^+$: 1860.0781, found: 1860.0753.

R12: White solid, yield = 37 mg, 81%. ^1H NMR (600 MHz, *v*/*v* = 1:2 $CDCl_3/CD_3CN$, 298 K) δ 8.06 (d, *J* = 7.8 Hz, 2H), 7.60 (t, *J* = 7.8 Hz, 2H), 7.39 (s, 1H), 7.33 (d, *J* = 7.8 Hz, 2H), 7.25–7.22 (m, 12H), 7.12–7.08 (m, 12H), 7.03 (d, *J* = 8.4 Hz, 4H), 6.99–6.96 (m, 4H), 6.58 (d, *J* = 8.4 Hz, 4H), 6.50 (d, *J* = 9.0 Hz, 2H), 6.44 (d, *J* = 8.4 Hz, 2H), 4.53 (s, 4H), 4.50 (s, 4H), 4.39 (s, 2H), 3.97 (t, *J* = 7.8 Hz, 2H), 3.78–3.73 (m, 6H), 3.49–3.46 (m, 4H), 1.81 (p, *J* = 6.0 Hz, 2H), 1.57 (p, *J* = 6.6 Hz, 4H), 1.49 (p, *J* = 7.8 Hz, 2H), 1.33–1.31 (m, 2H), 1.27–1.26 (m, 58H), 1.16–1.14 (m, 12H), 1.07–1.05 (m, 2H), 0.99–0.96 (m, 2H). ^{13}C NMR (151 MHz, *v*/*v* = 1:2 $CDCl_3/CD_3CN$, 298 K) δ 159.6, 159.3, 157.8, 157.7, 149.4, 145.6, 145.6, 140.4, 140.2, 132.7, 132.7, 131.5, 131.5, 131.0, 130.9, 130.8, 125.4, 123.8, 123.2, 120.8, 115.4, 114.2, 114.2, 73.0, 72.8, 68.5, 68.3, 67.9, 65.6, 65.1, 64.1, 64.1, 50.8, 35.2, 32.0, 30.9, 30.5, 30.3, 29.8, 29.7, 28.0, 26.9, 26.7, 26.2. IR (cm^{-1}): 2957, 2928, 2859, 1609, 1578, 1506, 1471, 1438, 1391, 1361, 1297, 1244, 1174, 1108, 1077, 1018, 821, 788, 704, 624, 579. HRMS (ESI+): *m/z* calcd. for $C_{124}H_{154}N_5O_7$ $[M+H]^+$: 1826.1876, found: 1826.1859.

[Cu(**R12**)](PF_6): Orange solid, yield = 19 mg, 92%. ^{1}H NMR (600 MHz, CD_3CN, 298 K) δ 8.12 (d, *J* = 8.0 Hz, 2H), 7.99 (t, *J* = 7.9 Hz, 2H), 7.70 (d, *J* = 7.7 Hz, 2H), 7.52 (s, 1H), 7.27 (dd, *J* = 8.7, 1.9 Hz, 12H), 7.15–7.08 (m, 16H), 6.93 (d, *J* = 8.6 Hz, 4H), 6.72 (d, *J* = 8.9 Hz, 2H), 6.64 (dd, *J* = 8.8, 2.0 Hz, 6H), 4.56–4.47 (m, 4H), 4.43 (s, 4H), 3.97 (d, *J* = 6.7 Hz, 4H), 3.86– 3.80 (m, 6H), 3.76 (t, *J* = 6.3 Hz, 2H), 3.19 (t, *J* = 6.1 Hz, 2H), 1.67 (q, *J* = 6.5 Hz, 6H), 1.56 (td, *J* = 7.7, 3.0 Hz, 4H), 1.45–1.40 (m, 4H), 1.31 (d, *J* = 7.4 Hz, 14H), 1.26 (d, *J* = 1.1 Hz, 54H), 1.12–1.08 (m, 2H). $^{13}C\{^1H\}$ NMR (151 MHz, CD_3CN, 298 K) δ 159.6, 158.8, 149.4, 145.5, 145.5, 139.9, 132.6, 132.6, 131.2, 130.2, 125.4, 115.0, 114.2, 114.2, 72.6, 71.7, 68.6, 68.3, 67.8, 65.4, 63.9, 51.3, 34.9, 31.5, 30.3, 30.0, 29.8, 29.7, 29.6, 29.5, 29.4, 26.6, 26.5, 25.9. IR (cm^{-1}): 2953, 2924, 2859, 1609, 1578, 1506, 1465, 1393, 1361, 1300, 1246, 1176, 1103, 1081, 1018, 839, 823, 704, 624, 579, 556, 525. HRMS (ESI+): *m/z* calcd. for $C_{124}H_{153}N_5O_7Cu$ $[M\text{-}PF_6]^+$: 1889.1100, found: 1889.1059.

1.2 NMR Characterisations.

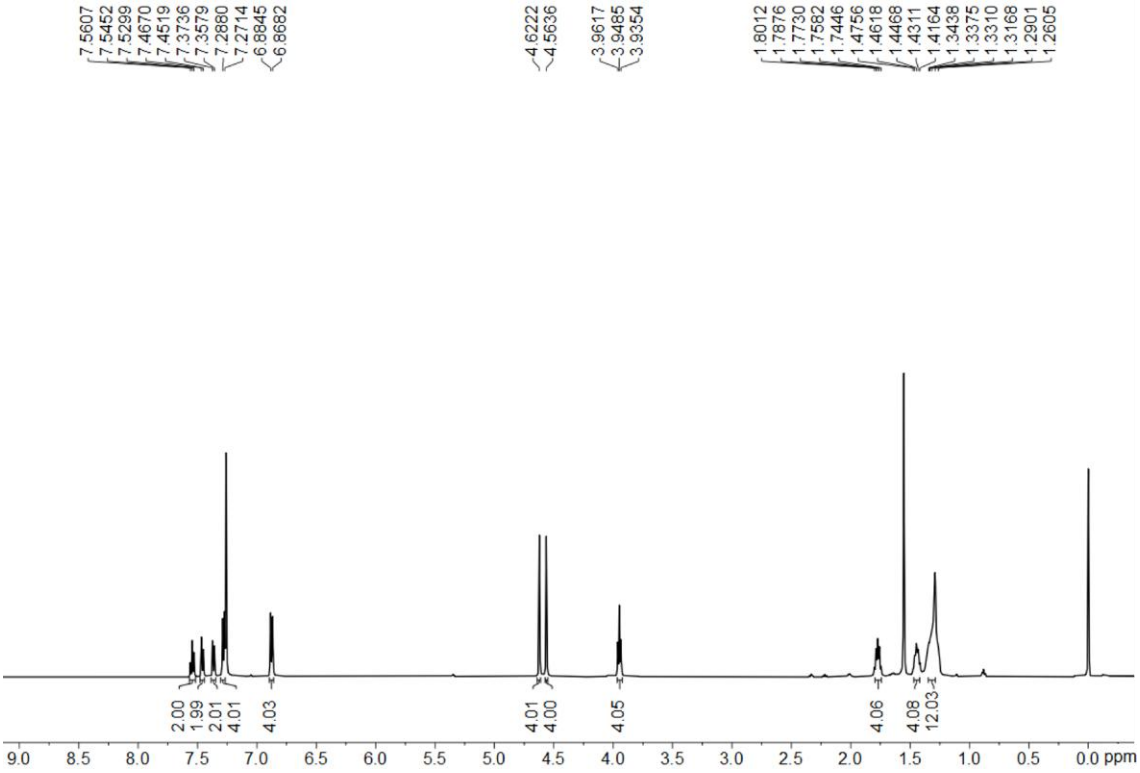

Fig. S1. ^{1}H NMR (500 MHz, CD_3CN, 298 K) spectrum of **2**.

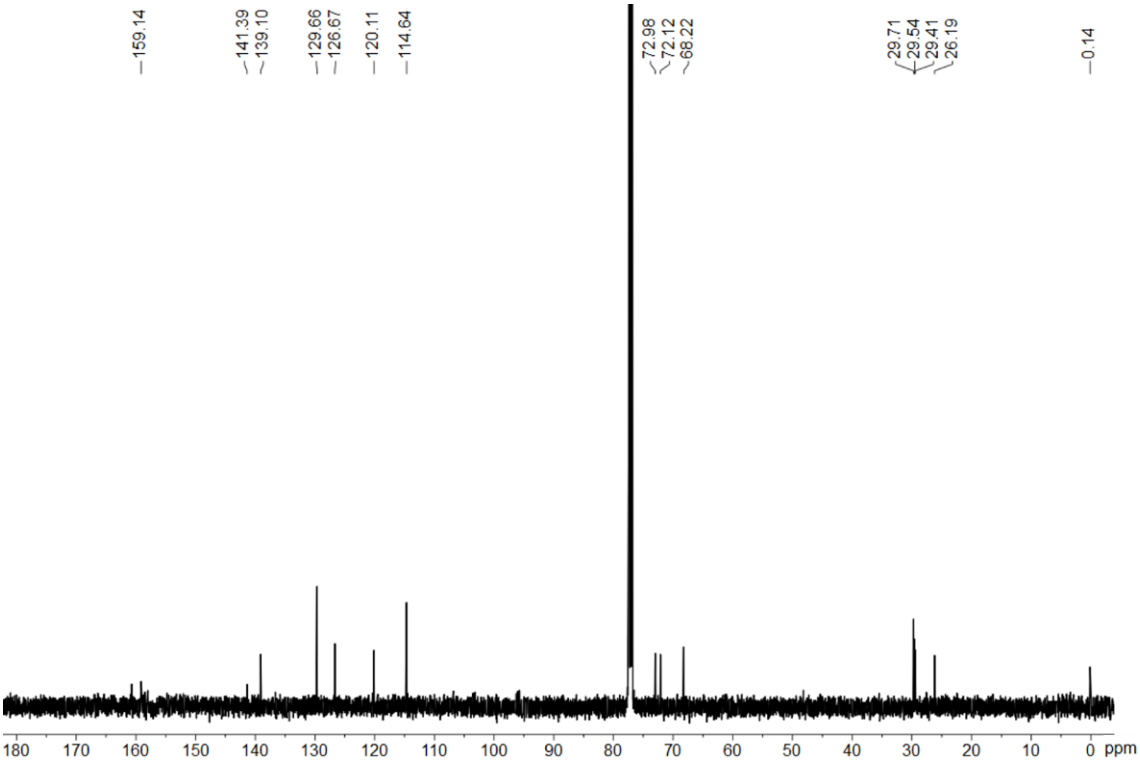

Fig. S2. $^{13}C\{^{1}H\}$ NMR (126 MHz, CD_3CN, 298 K) spectrum of **2.**

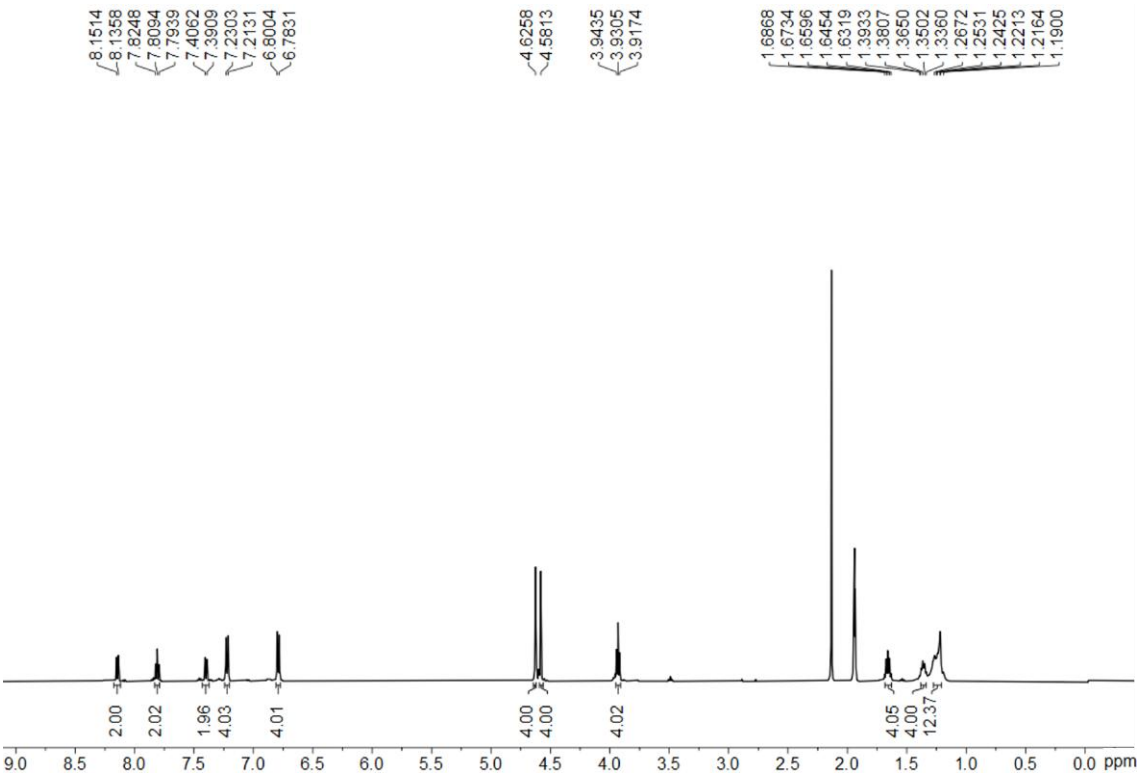

Fig. S3. ^{1}H NMR (500 MHz, CD_3CN, 298 K) spectrum of **M12**.

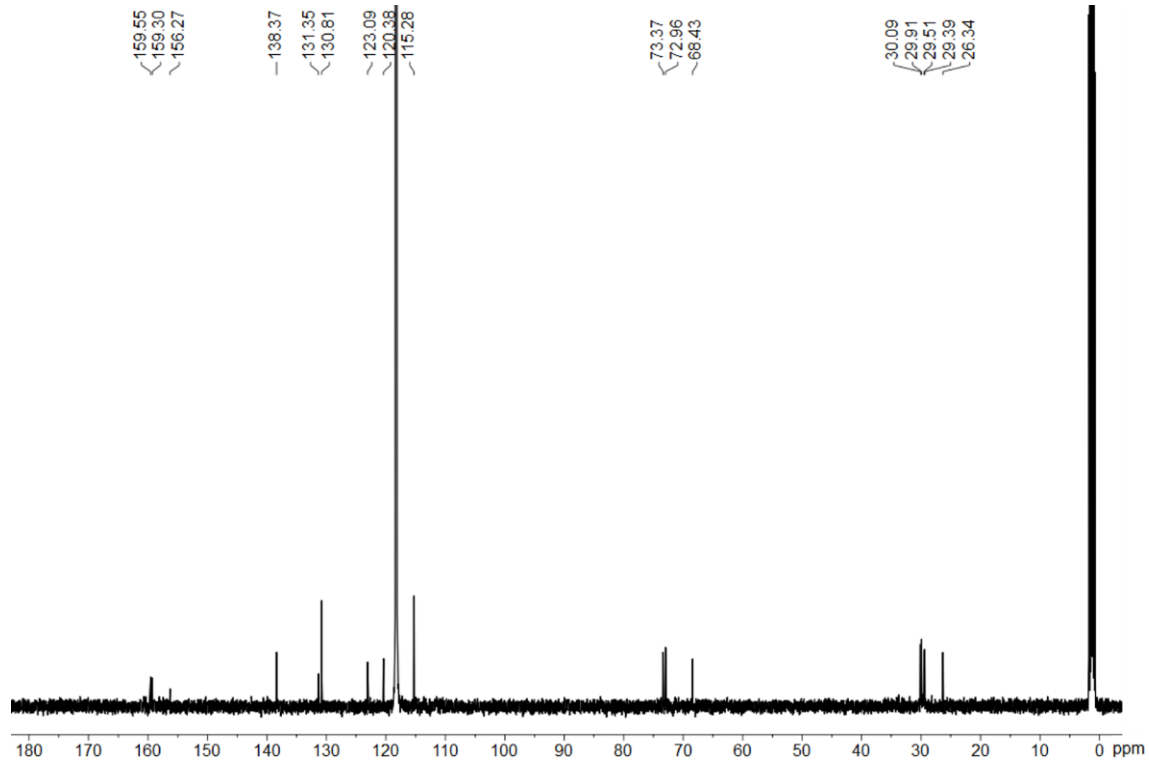

Fig. S4. $^{13}C\{^{1}H\}$ NMR (126 MHz, CD_3CN, 298 K) spectrum of **M12**.

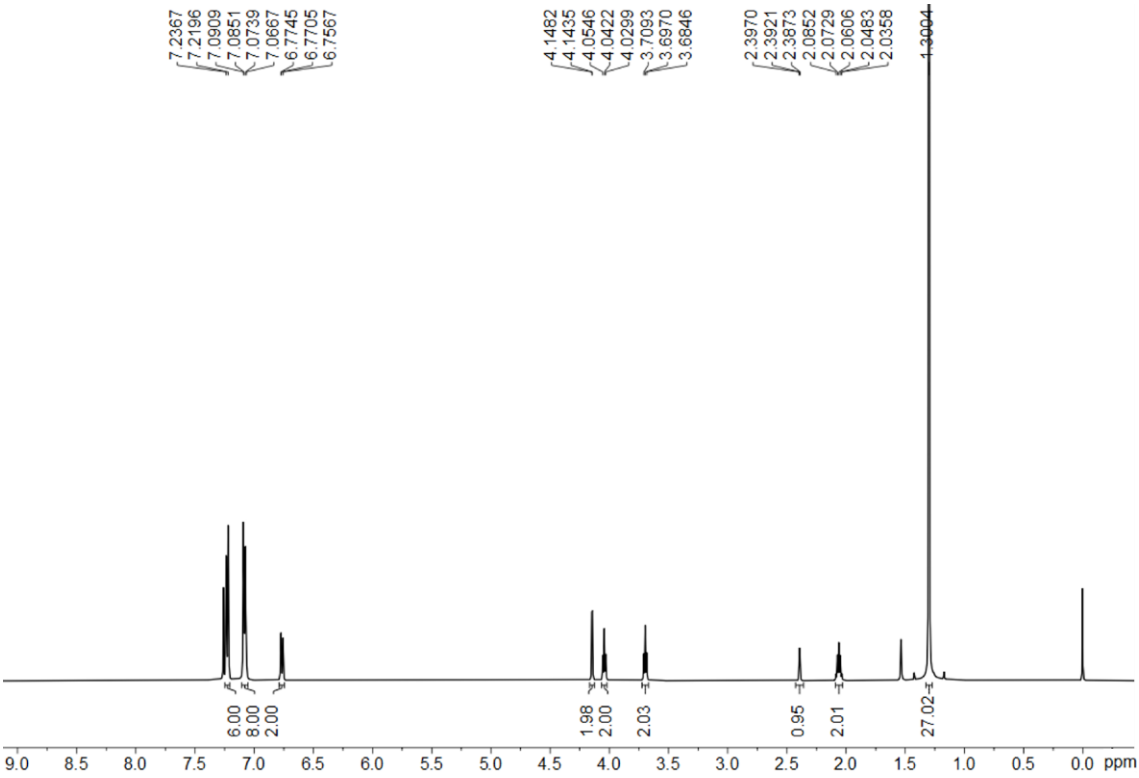

Fig. S5. ^{1}H NMR (500 MHz, $CDCl_3$, 298 K) spectrum of **4**.

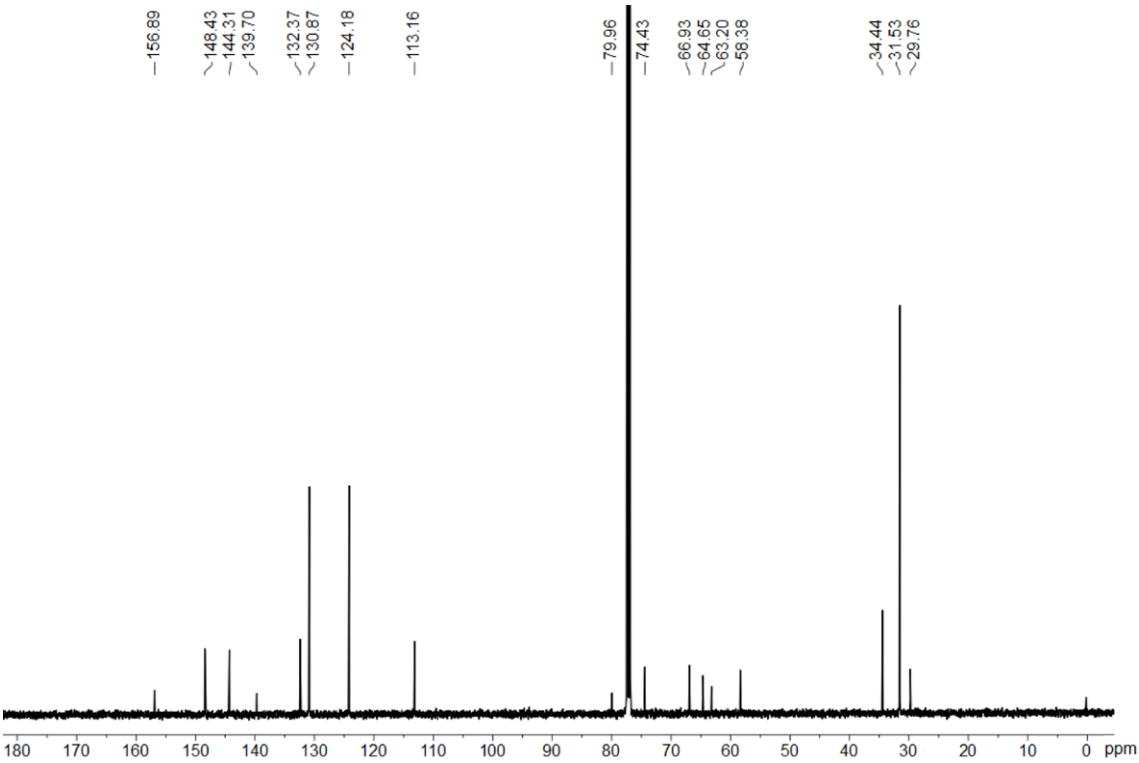

Fig. S6. ^{13}C{^{1}H} NMR (126 MHz, $CDCl_3$, 298 K) spectrum of **4**.

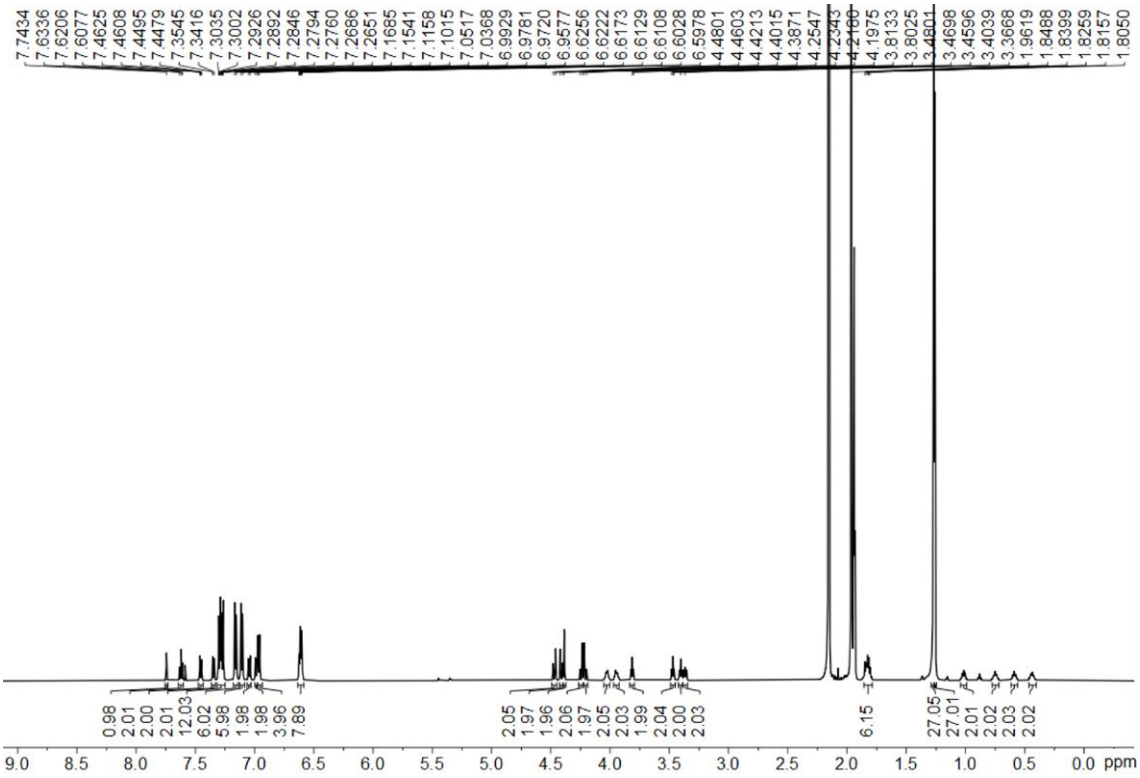

Fig. S7. ^{1}H NMR (600 MHz, *v*/*v* = 1:2 $CDCl_3/CD_3CN$, 298 K) spectrum of **R4**.

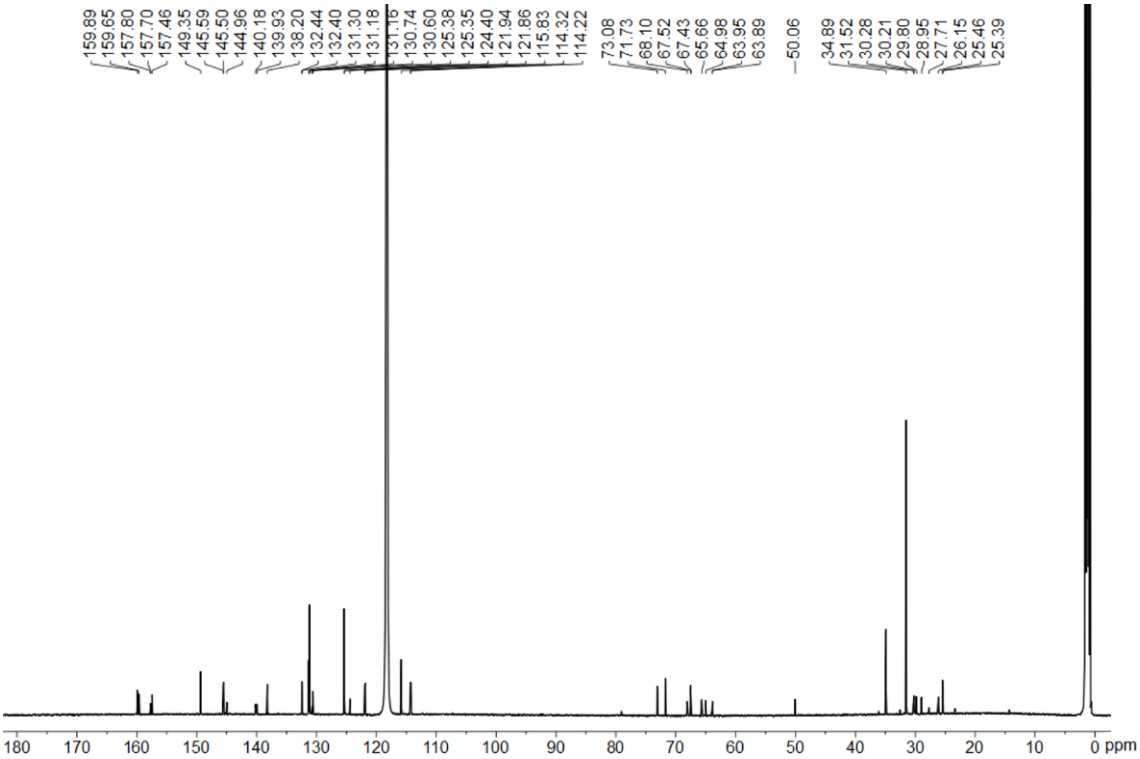

Fig. S8. $^{13}C\{^{1}H\}$ NMR (151 MHz, *v*/*v* = 1:2 $CDCl_3/CD_3CN$, 298 K) spectrum of **R4**.

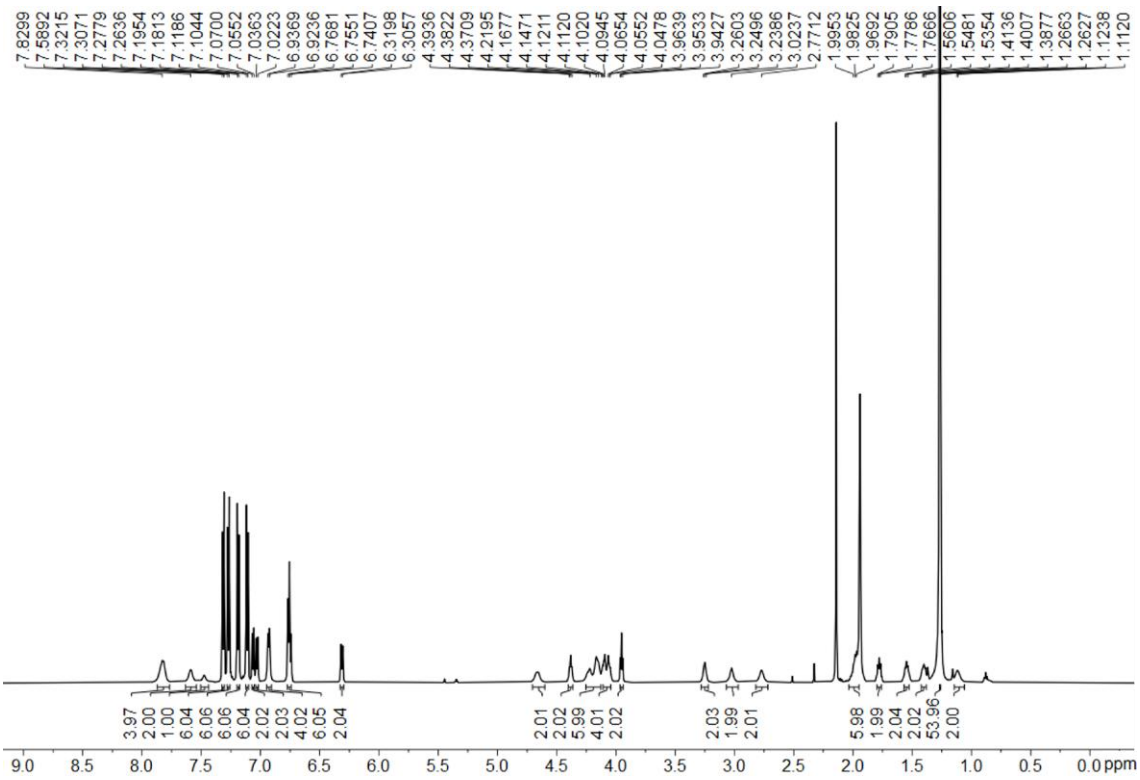

Fig. S9. ^{1}H NMR (600 MHz, CD_3CN, 298 K) spectrum of [Cu(**R4**)](PF_6).

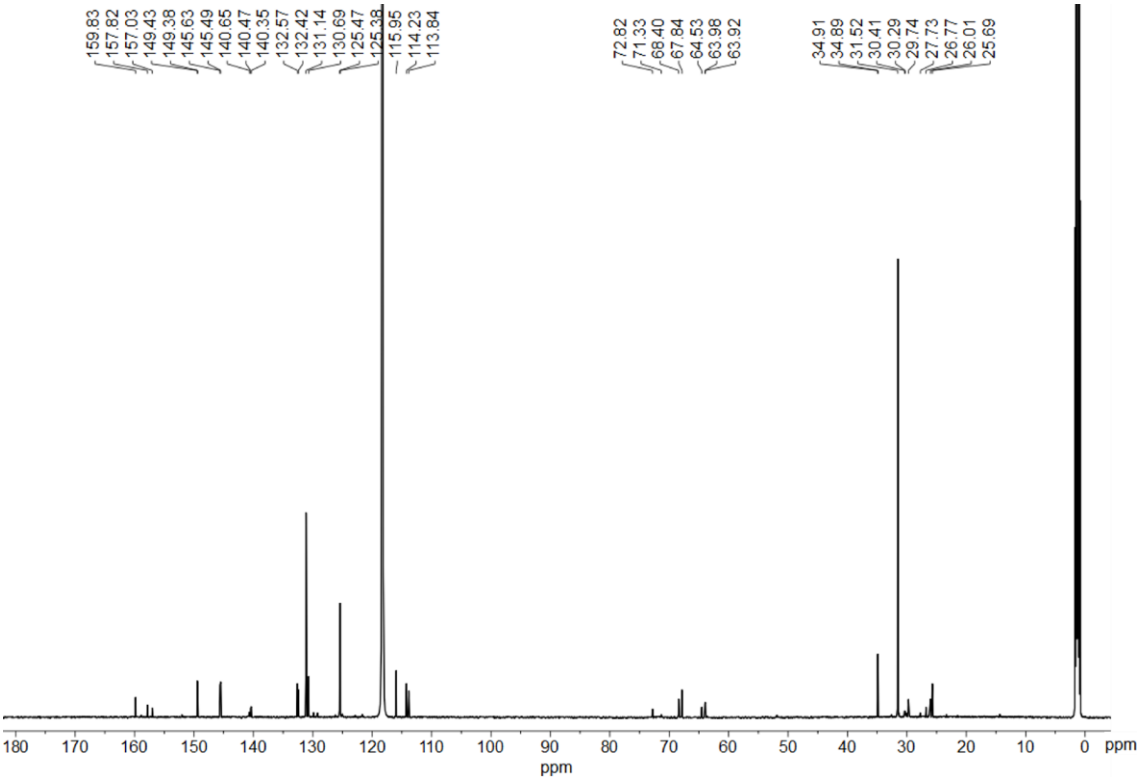

Fig. S10. $^{13}C\{^{1}H\}$ NMR (151 MHz, CD_3CN, 298 K) spectrum of [Cu(**R4**)](PF_6).

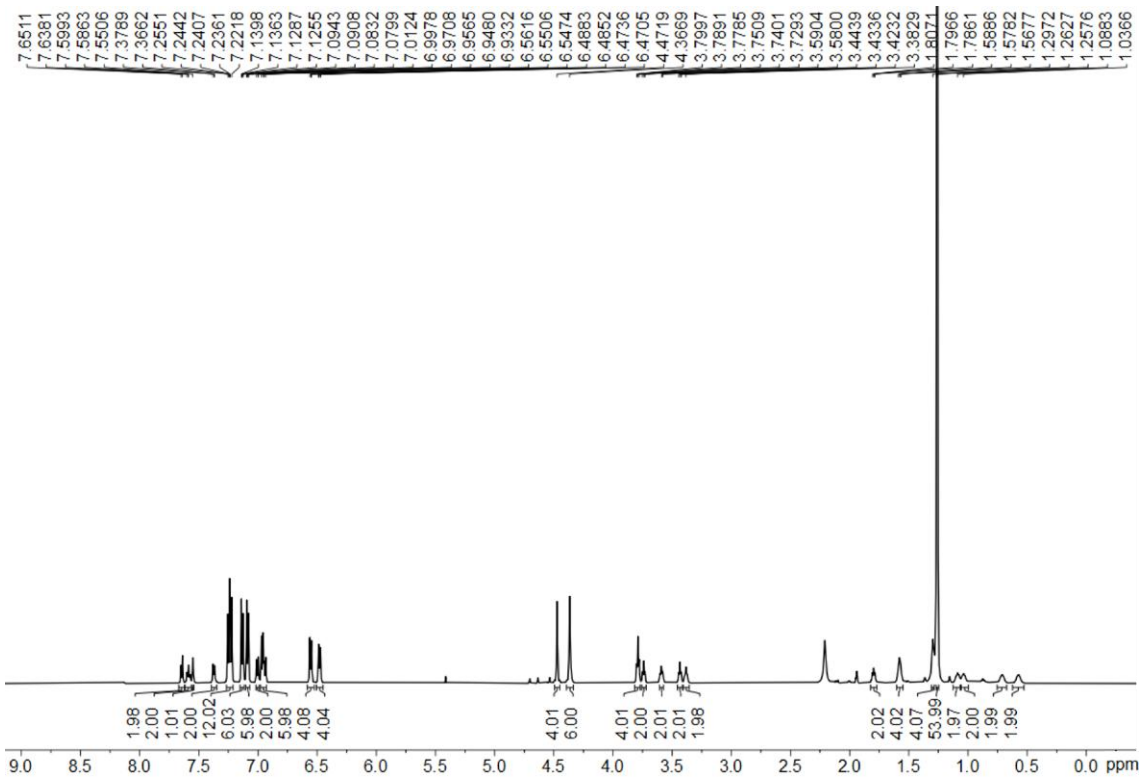

Fig. S11. ^{1}H NMR (600 MHz, *v*/*v* = 1:2 $CDCl_3/CD_3CN$, 298 K) spectrum of **R6**.

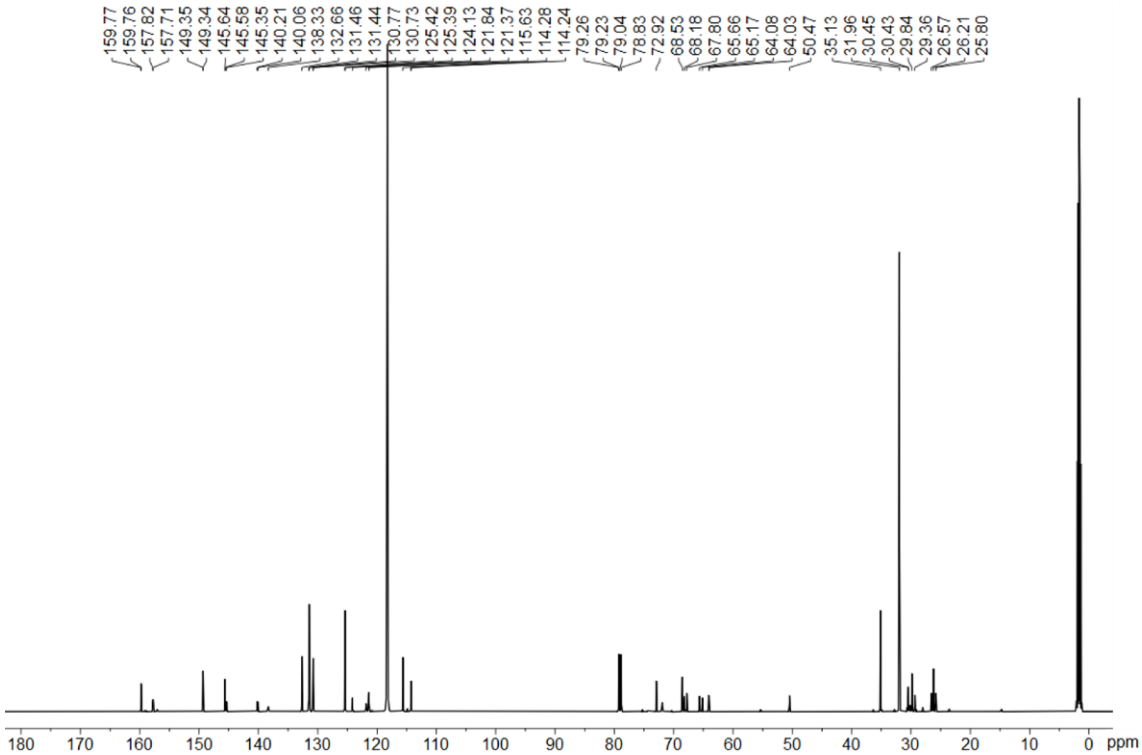

Fig. S12. $^{13}C\{^{1}H\}$ NMR (151 MHz, *v*/*v* = 1:2 $CDCl_3/CD_3CN$, 298 K) spectrum of **R6**.

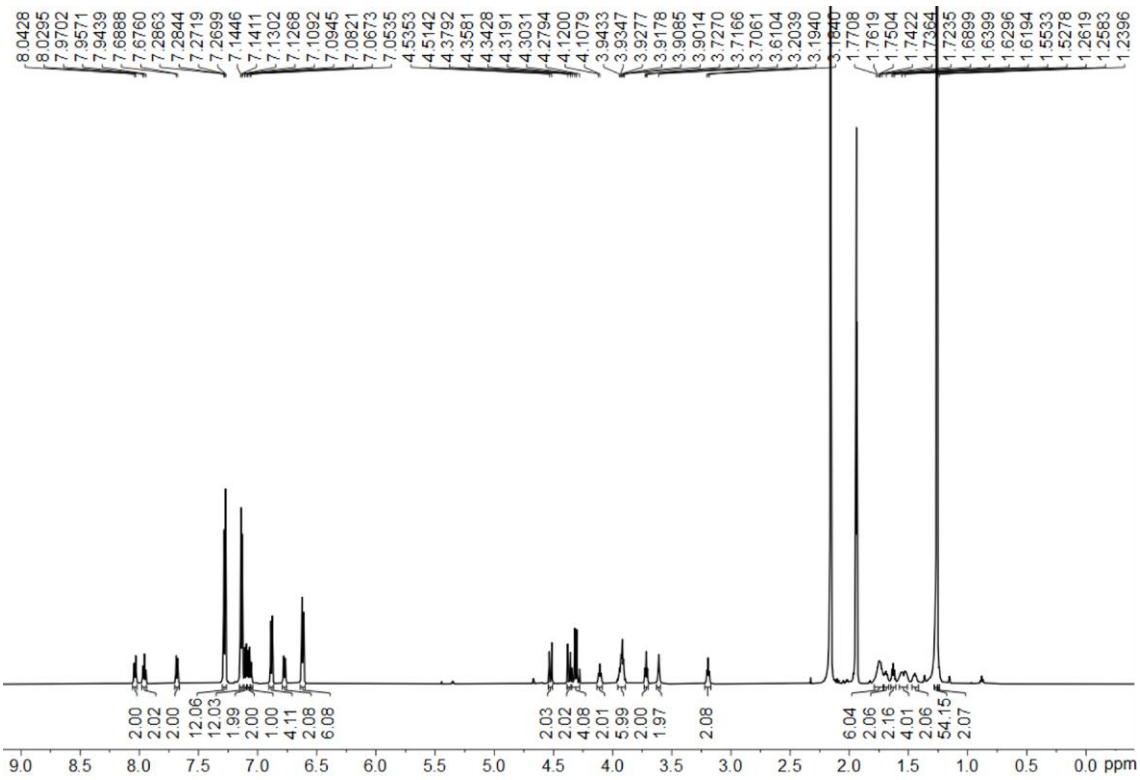

Fig. S13. ^{1}H NMR (600 MHz, CD_3CN, 298 K) spectrum of [Cu(**R6**)](PF_6).

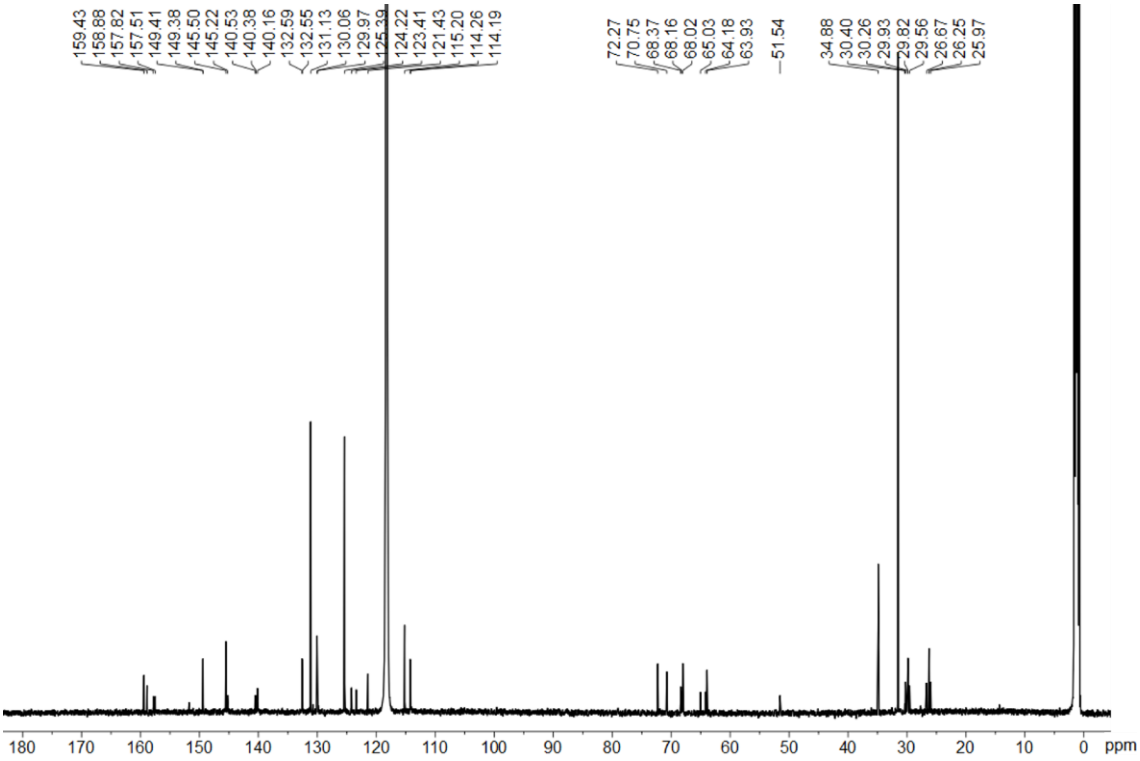

Fig. S14. $^{13}C\{^{1}H\}$ NMR (151 MHz, CD_3CN, 298 K) spectrum of [Cu(**R6**)](PF_6).

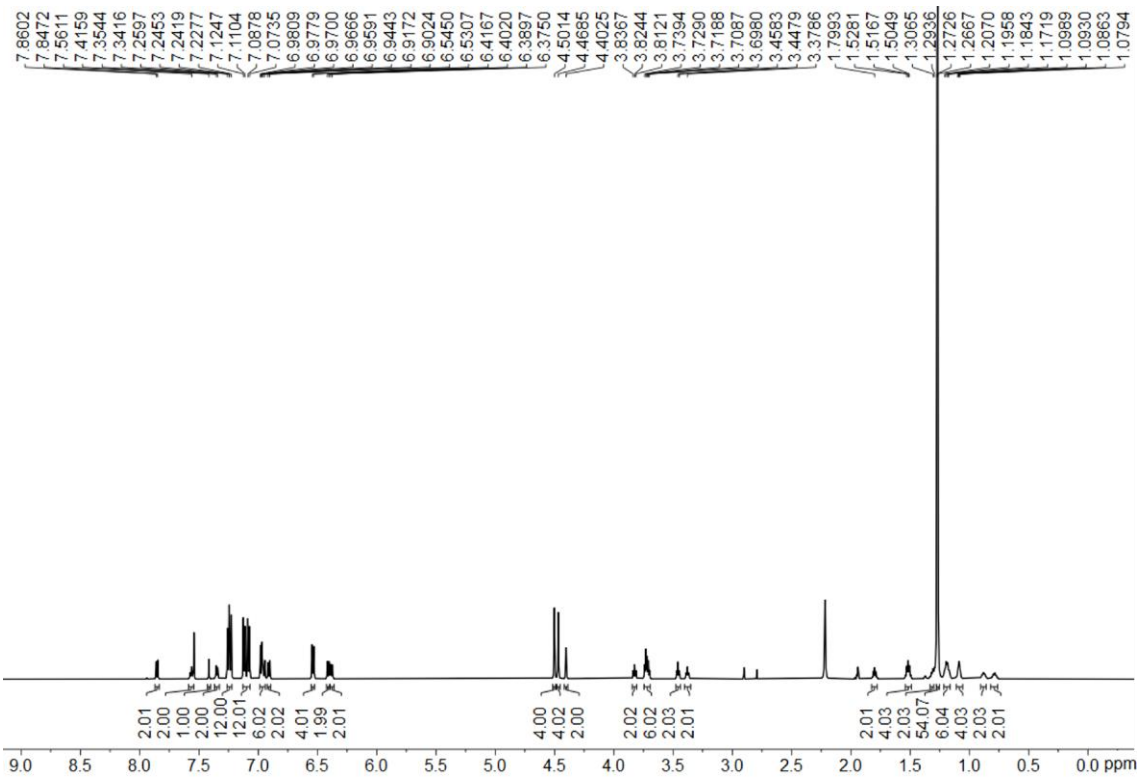

Fig. S15. ^{1}H NMR (600 MHz, *v*/*v* = 1:2 $CDCl_3/CD_3CN$, 298 K) spectrum of **R8**.

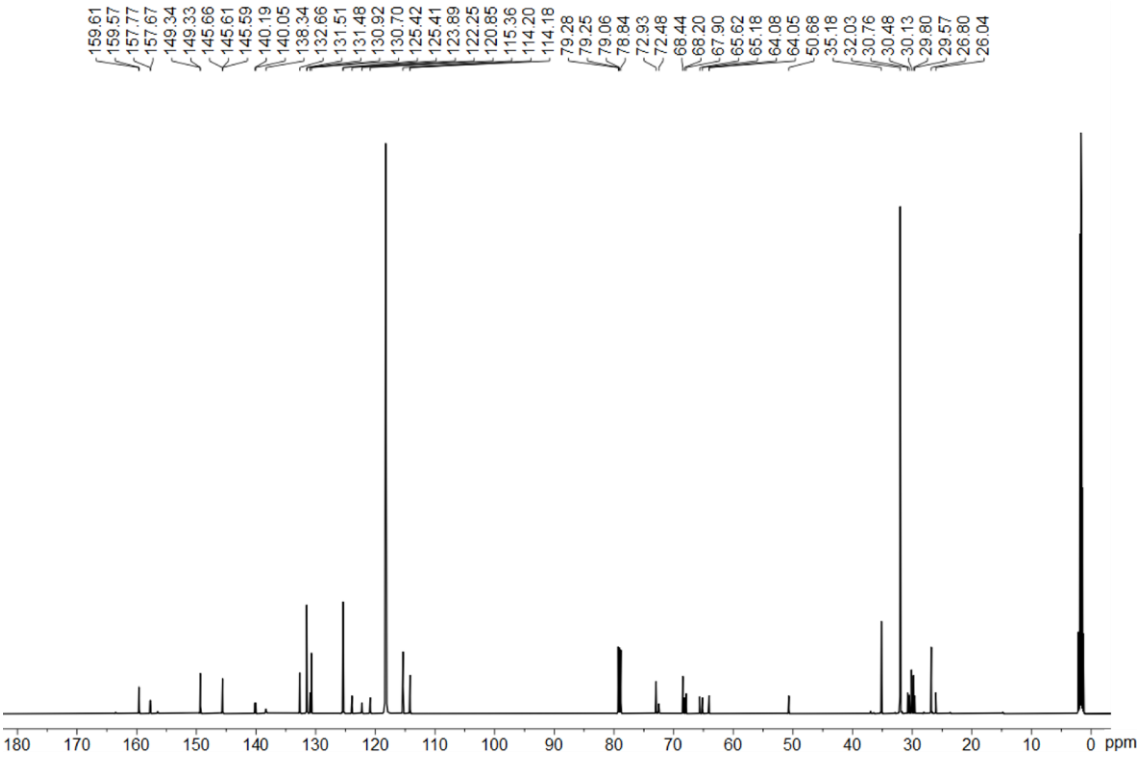

Fig. S16. $^{13}C\{^{1}H\}$ NMR (151 MHz, *v*/*v* = 1:2 $CDCl_3/CD_3CN$, 298 K) spectrum of **R8**.

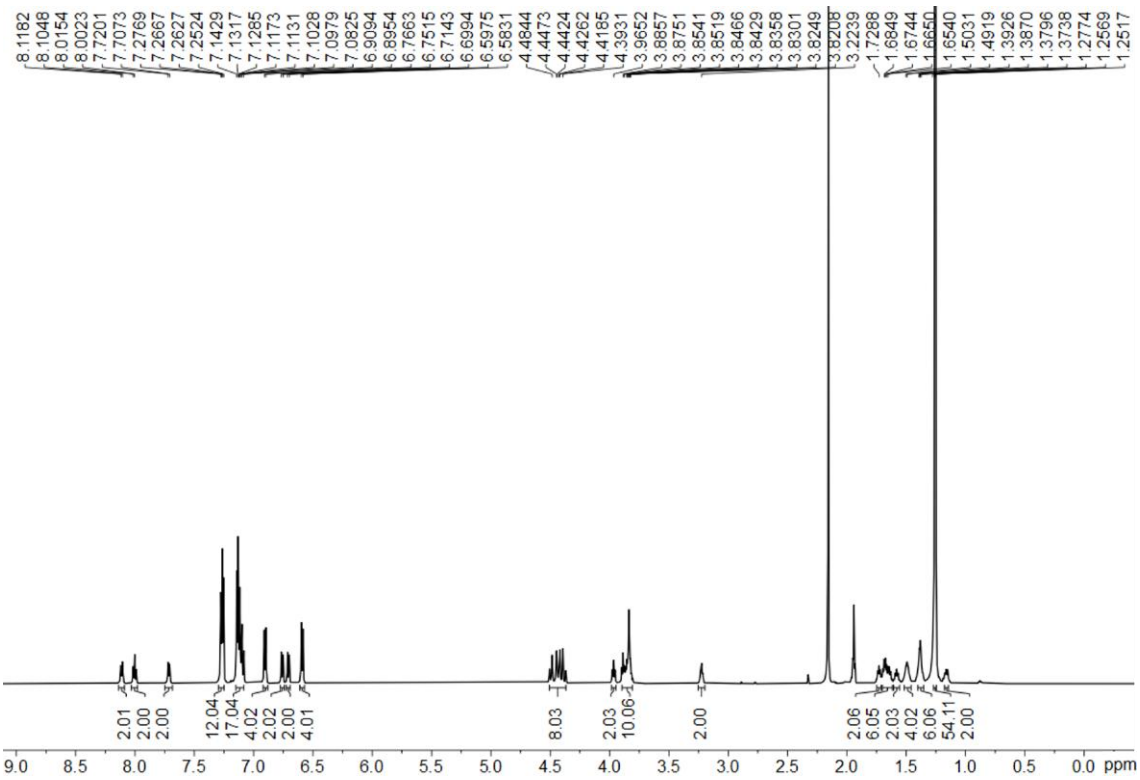

Fig. S17. ^{1}H NMR (600 MHz, CD_3CN, 298 K) spectrum of [Cu(**R8**)](PF_6).

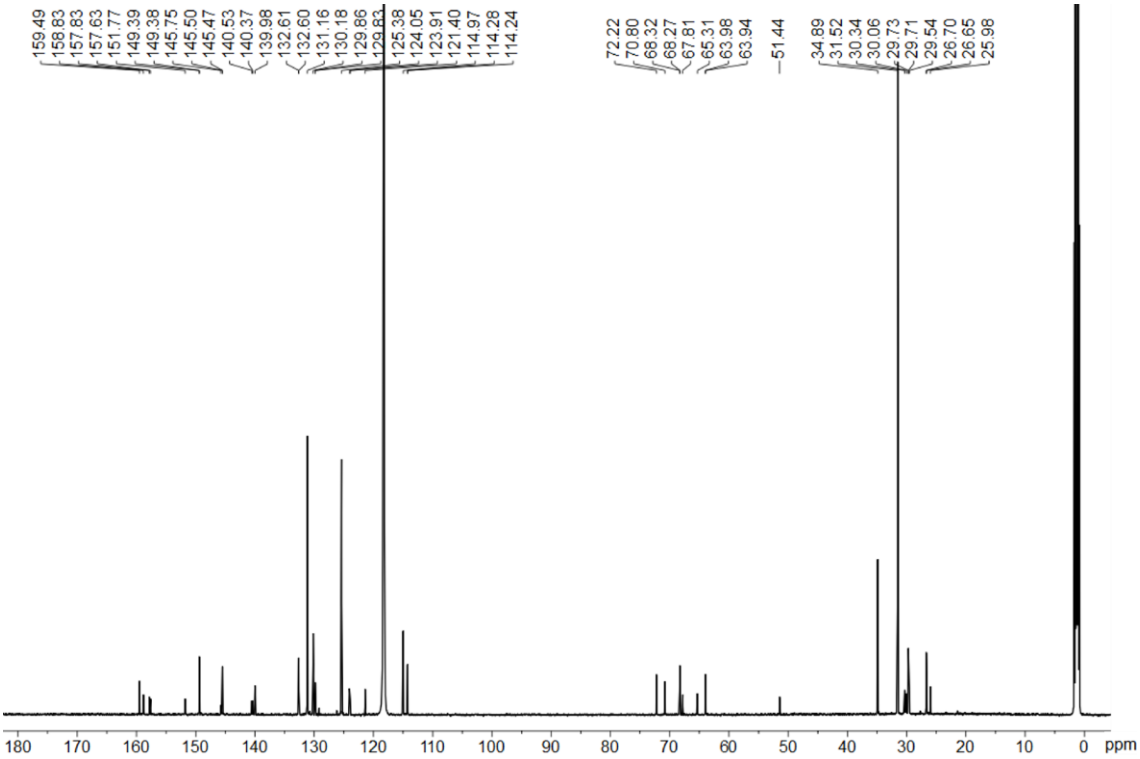

Fig. S18. $^{13}C\{^{1}H\}$ NMR (151 MHz, CD_3CN, 298 K) spectrum of [Cu(**R8**)](PF_6).

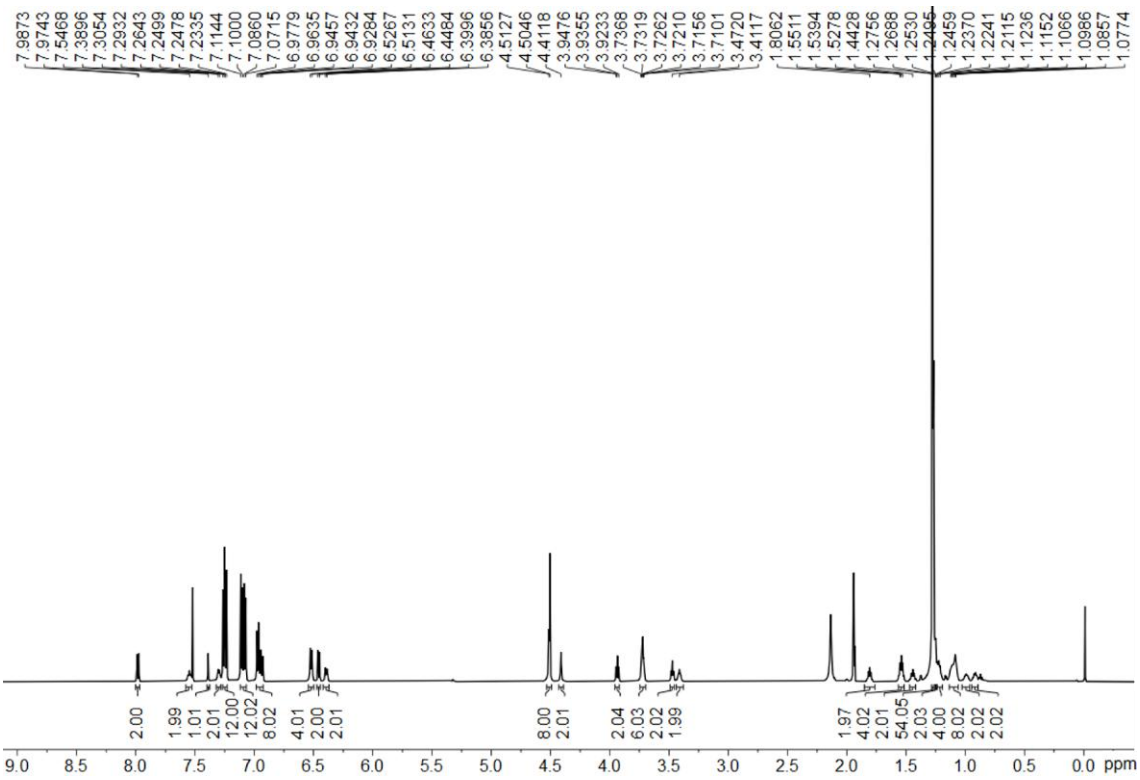

Fig. S19. ^{1}H NMR (600 MHz, *v*/*v* = 1:2 $CDCl_3/CD_3CN$, 298 K) spectrum of **R10**.

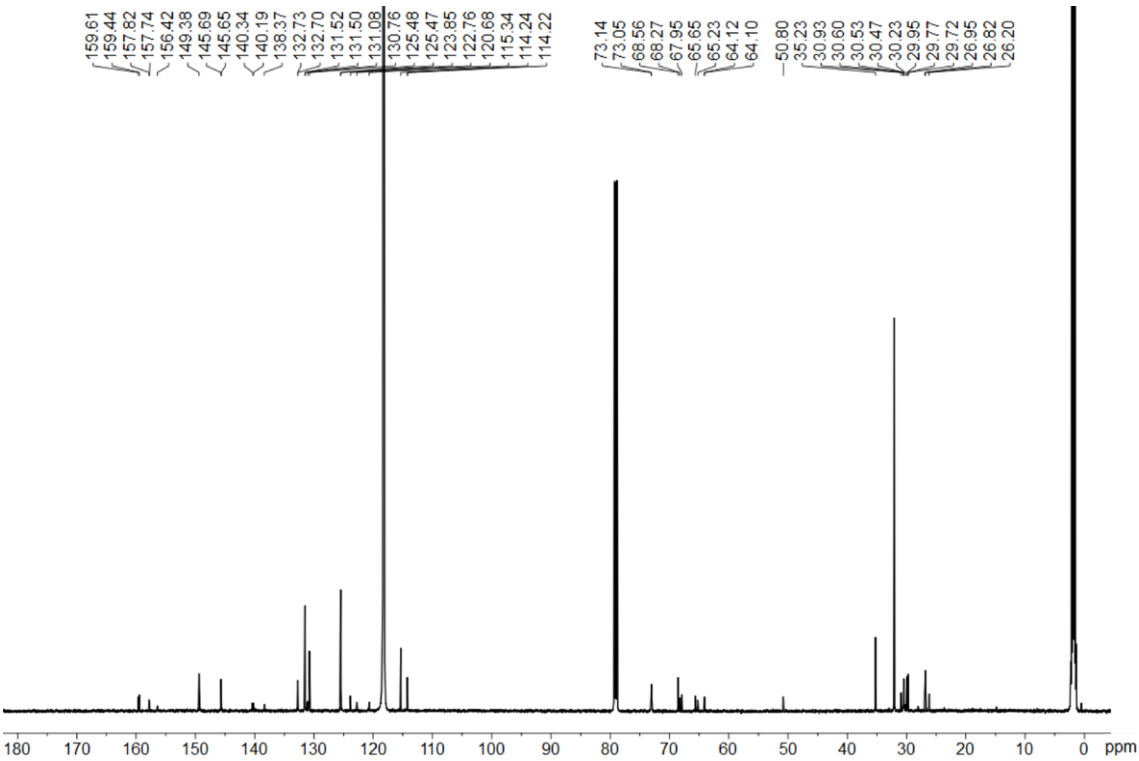

Fig. S20. $^{13}C\{^{1}H\}$ NMR (151 MHz, *v*/*v* = 1:2 $CDCl_3/CD_3CN$, 298 K) spectrum of **R10**.

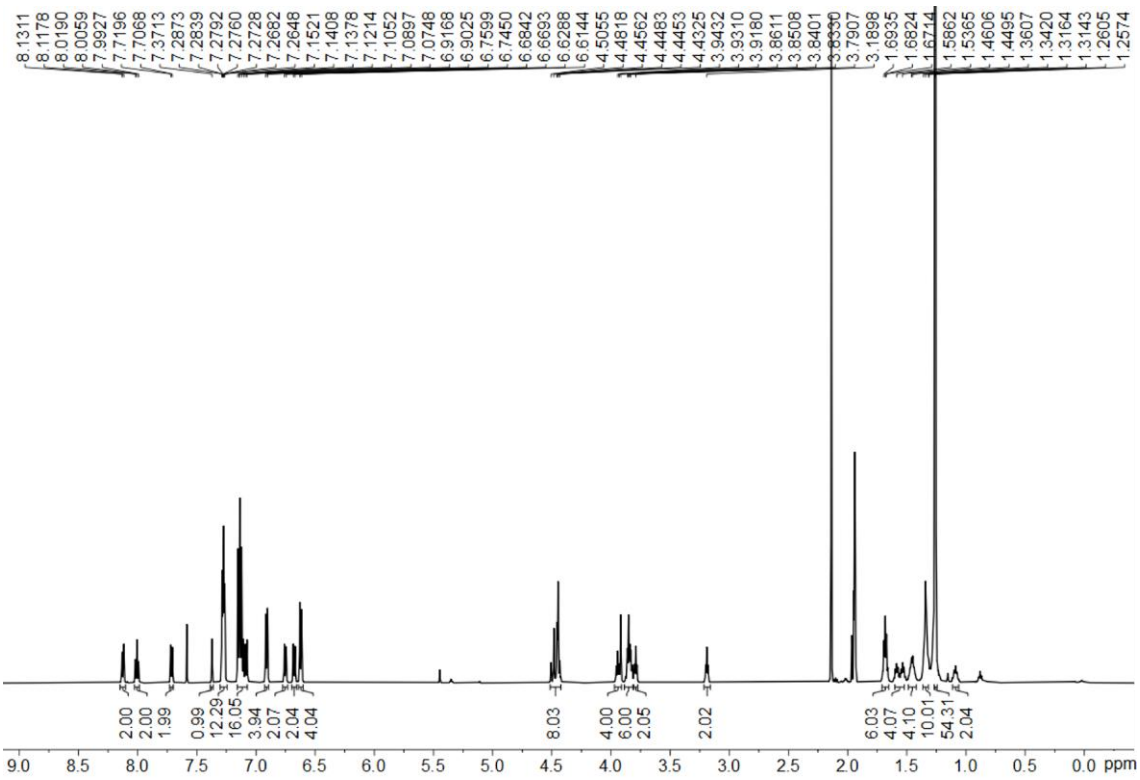

Fig. S21. ^{1}H NMR (600 MHz, CD_3CN, 298 K) spectrum of [Cu(**R10**)](PF_6).

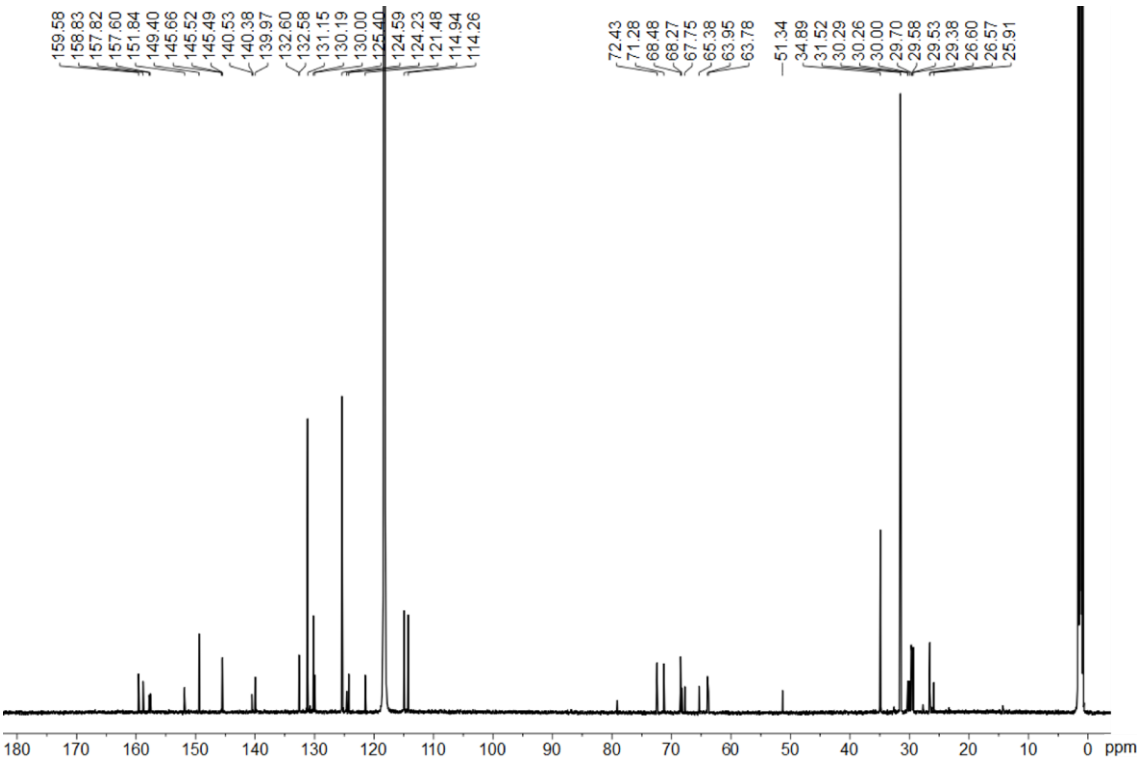

Fig. S22. $^{13}C\{^{1}H\}$ NMR (151 MHz, CD_3CN, 298 K) spectrum of [Cu(**R10**)](PF_6).

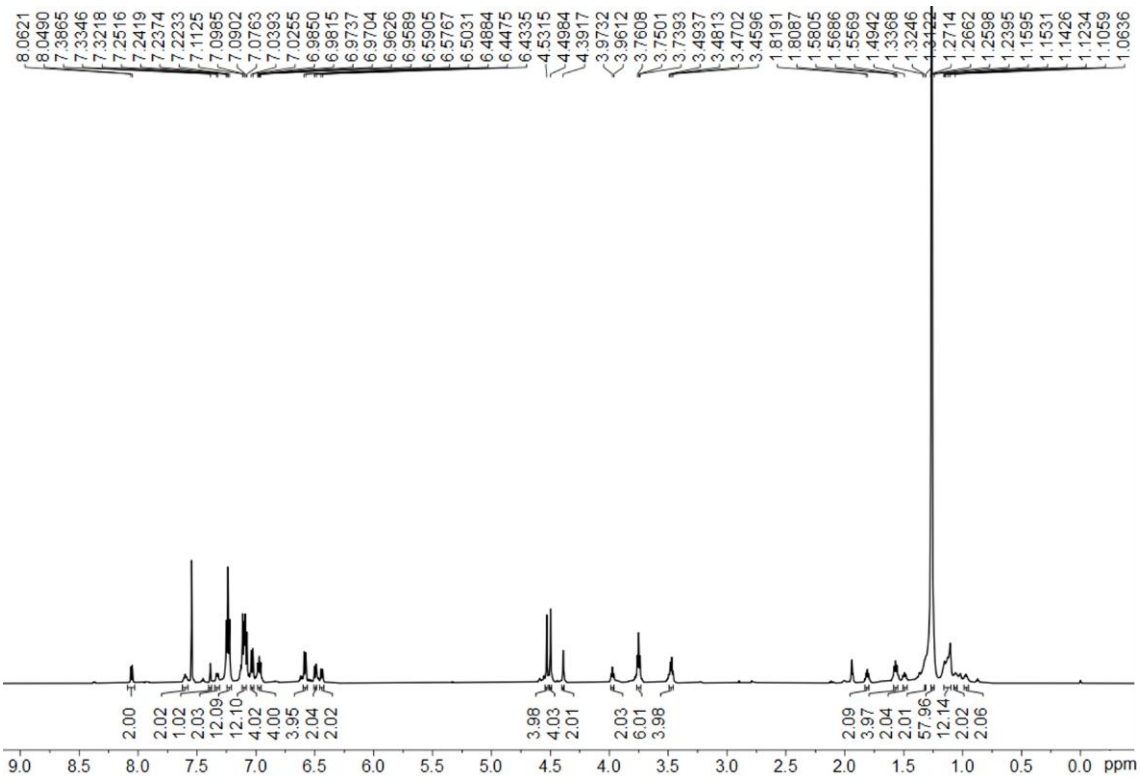

Fig. S23. ^{1}H NMR (600 MHz, *v*/*v* = 1:2 $CDCl_3$/CD_3CN, 298 K) spectrum of **R12**.

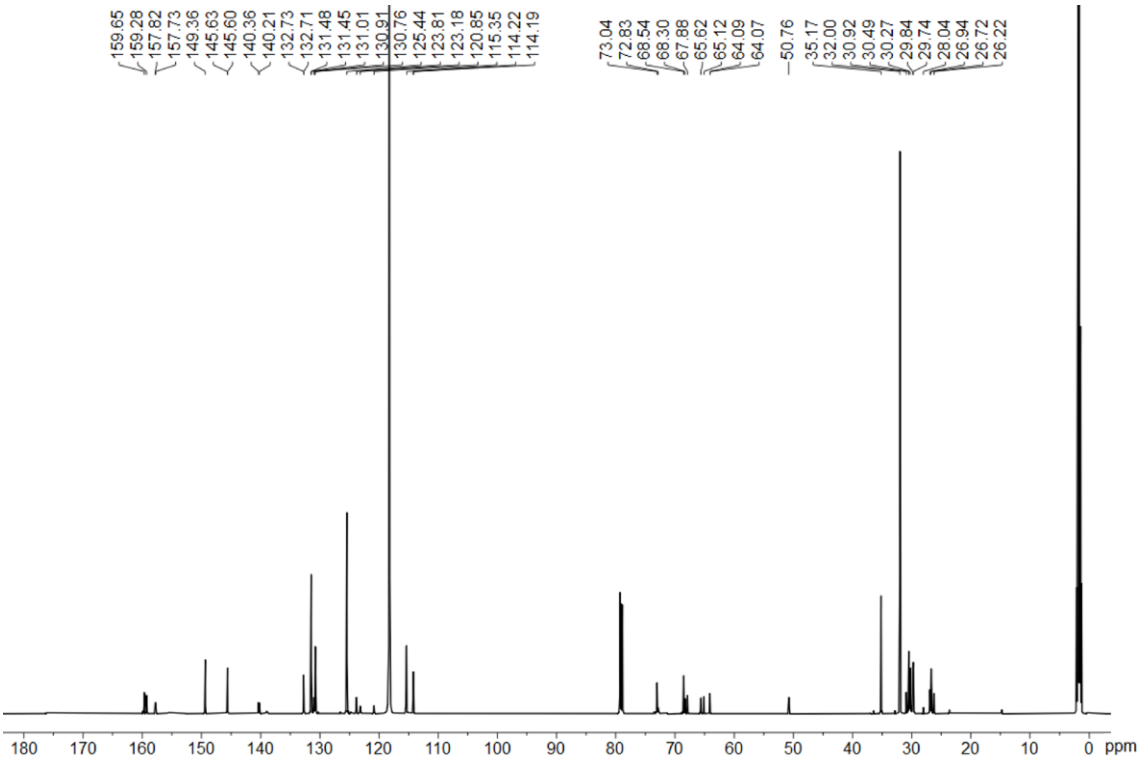

Fig. S24. $^{13}C\{^{1}H\}$ NMR (151 MHz, *v*/*v* = 1:2 $CDCl_3$/CD_3CN, 298 K) spectrum of **R12**.

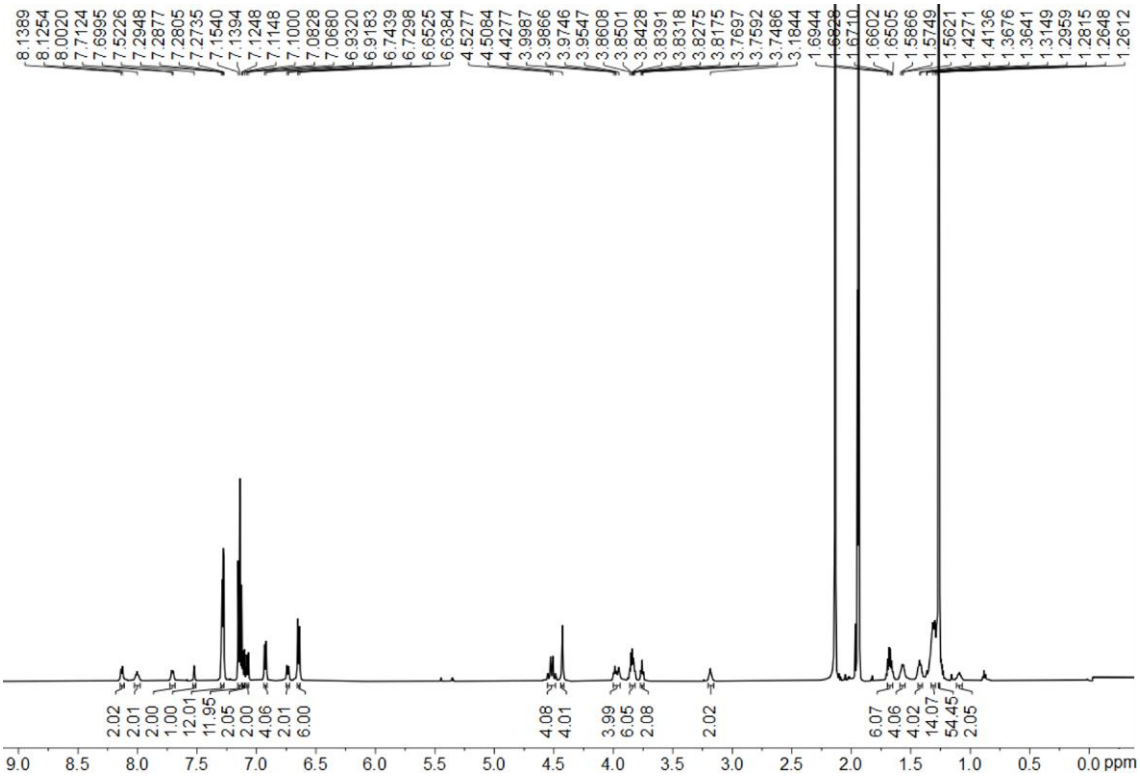

Fig. S25. ^{1}H NMR (600 MHz, CD_3CN, 298 K) spectrum of [Cu(**R12**)](PF_6).

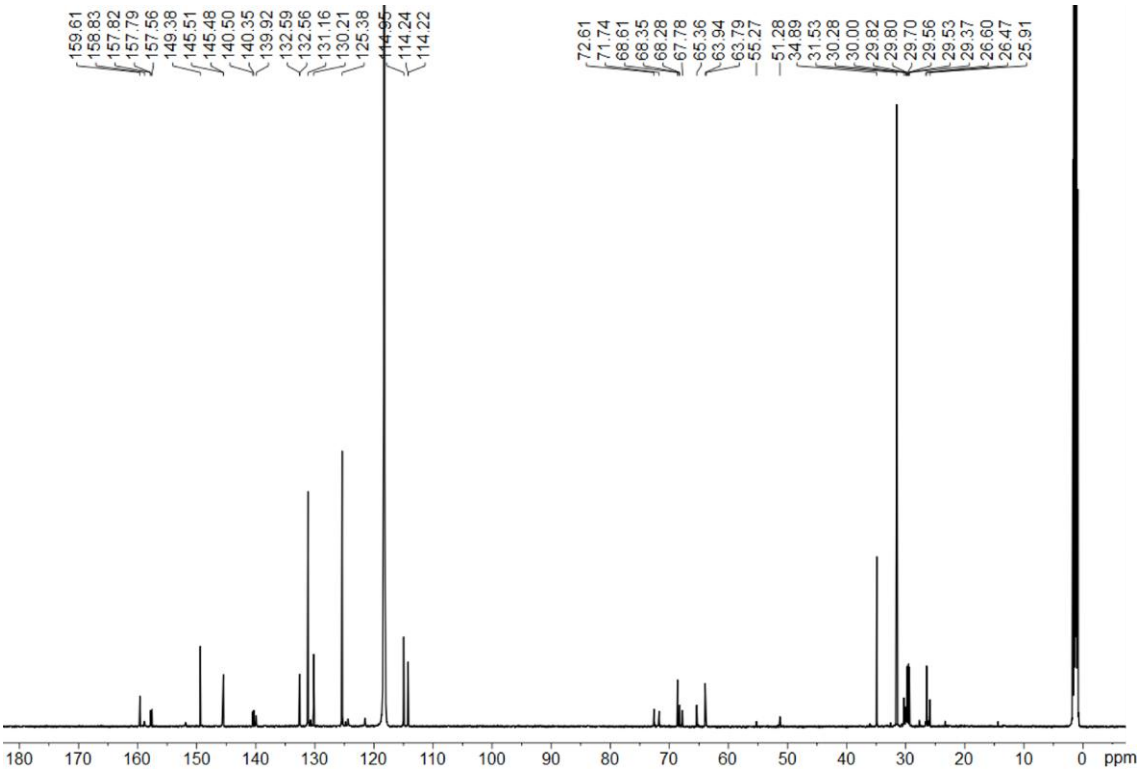

Fig. S26. $^{13}C\{^{1}H\}$ NMR (151 MHz, CD_3CN, 298 K) spectrum of [Cu(**R12**)](PF_6).

Table S1. Partial ^{1}H NMR shift analysis of the PF_6^- salts of $[Cu(\mathbf{Rn})]^+$, (n = 4, 6, 8, 10, 12).

	^{1}H NMR (ppm)						
	δH_6	δH_7	δH_8	δH_m	δH_p	δH_k	δH_n
$[Cu(\mathbf{R4})]^+$	6.93	6.77–6.74	4.12–4.04	3.02	3.25	4.38	2.77
$[Cu(\mathbf{R6})]^+$	6.88	6.64–6.61	3.95–3.90	3.61	3.95	4.11	3.19
$[Cu(\mathbf{R8})]^+$	6.90	6.59	3.95–3.81	3.83	3.88	3.97	3.22
$[Cu(\mathbf{R10})]^+$	6.91	6.62	3.89–3.81	3.85	3.79	3.94	3.19
$[Cu(\mathbf{R12})]^+$	6.93	6.64	3.86–3.80	3.96	3.76	3.98	3.19

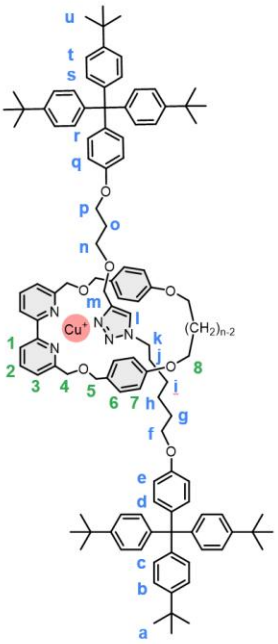

1.3 Mass Spectrometry.

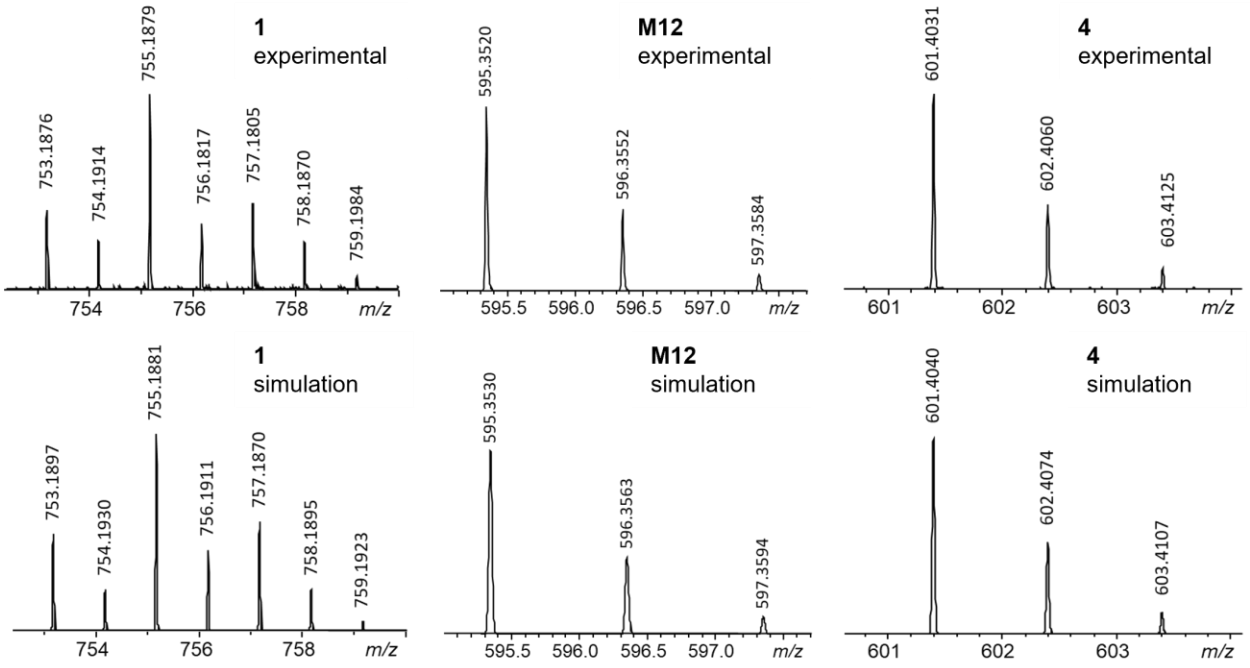

Fig. S27. HR-ESI-MS spectra of rotaxane precursors **1** (left), **M12** (middle) and **4** (right) reported in this work.

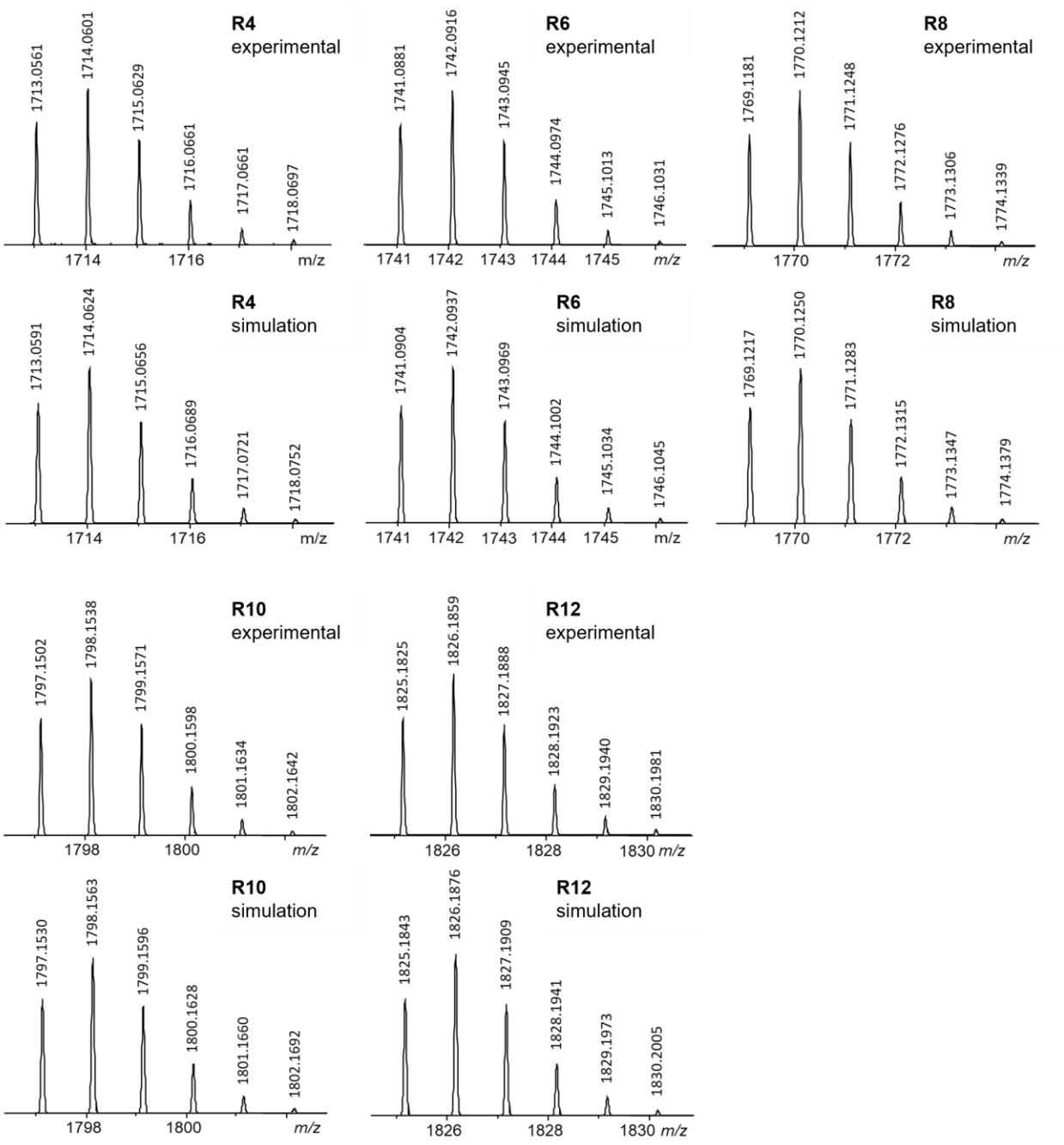

Fig. S28. HR-ESI-MS spectra of the [2]rotaxanes **R4**, **R6**, **R8**, **R10** and **R12**.

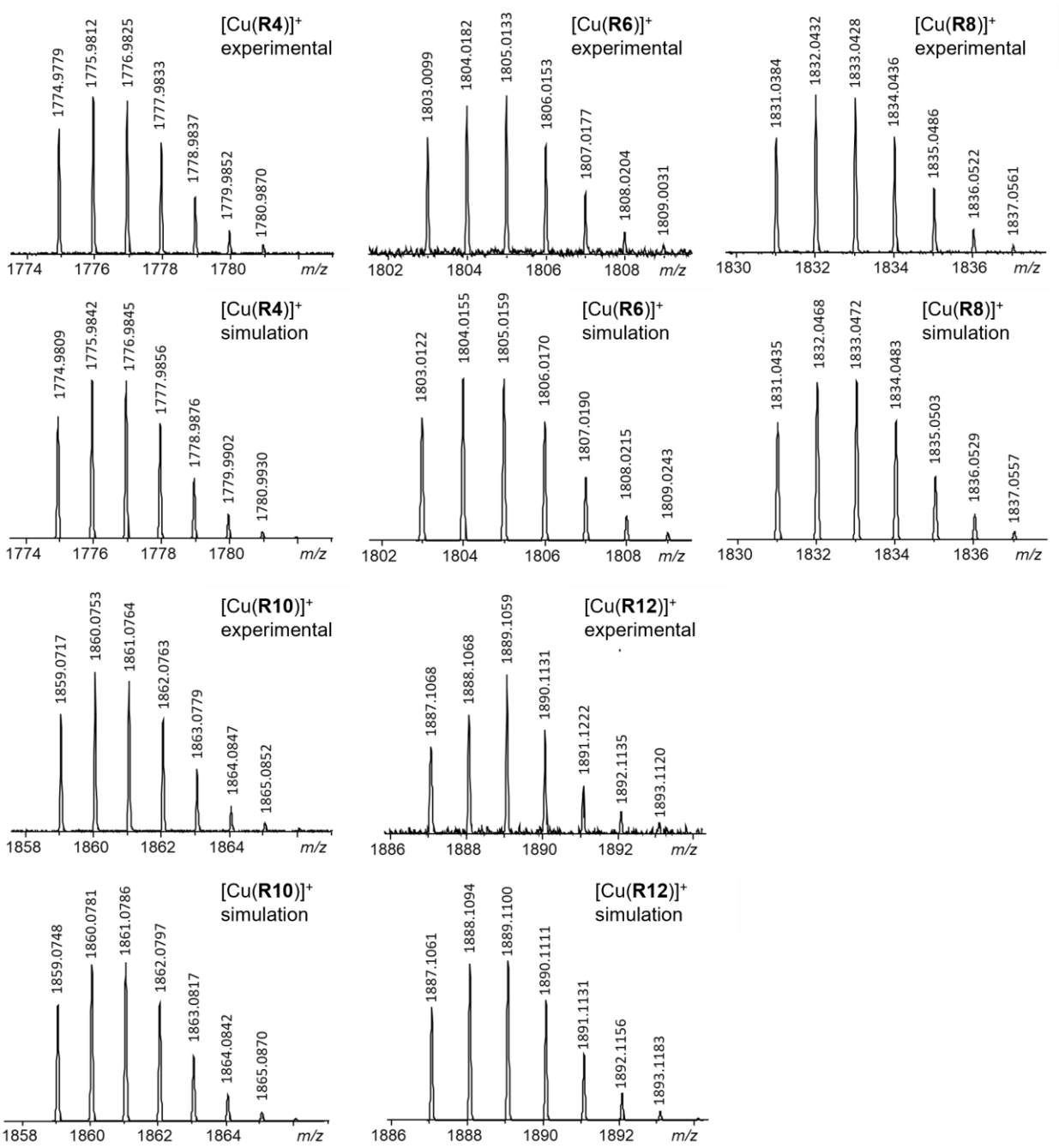

Fig. S29. HR-ESI-MS spectra of the Cu^{I} [2]rotaxane complexes [Cu(**R4**)]$^{+}$, [Cu(**R6**)]$^{+}$, [Cu(**R8**)]$^{+}$, [Cu(**R10**)]$^{+}$, and [Cu(**R12**)]$^{+}$.

1.4 X-ray Crystallography.

Bruker D8 VENTURE X-ray diffractometer was used for crystal screening, unit cell determination, and data collection for the X-ray crystal structure of [Cu(**R6**)](PF$_6$). Data was collected using a Mo Kα X-ray radiation (λ = 0.71073 Å) at 100 K. The ShelXT program was used to solve the structure, and *Olex2* was used for the graphical interface.[4] The models were refined with ShelXL 2014/7 (Sheldrick, 2015) using full matrix Least Squares minimisation on F^2. SQUEEZE routine in PLATON was employed in the structural refinements. The X-ray crystallographic coordinates have been deposited at CCDC, under the deposition number 2457336, 2504020. These data can be obtained free of charge from CCDC via https://www.ccdc.cam.ac.uk/structures/.

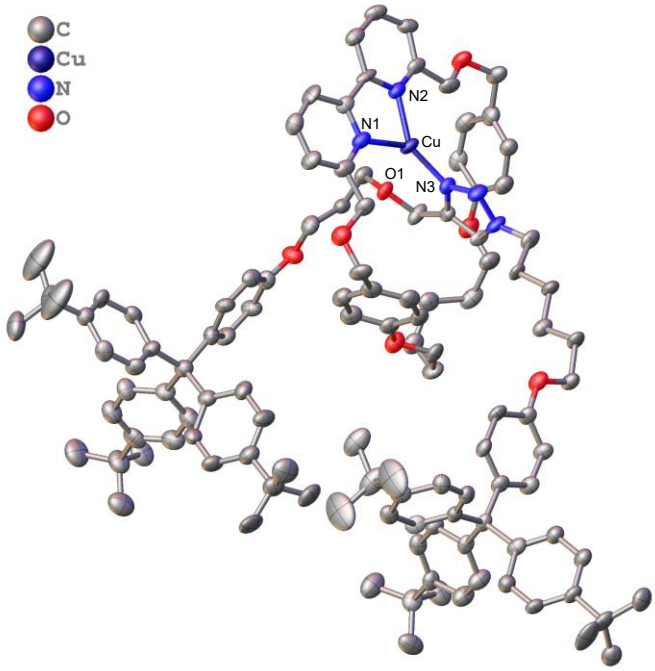

Fig. S30. Crystal structure of [Cu(**R6**)](PF$_6$) (CCDC: 2457336). All H atoms have been omitted for clarity. Thermal ellipsoids are scaled to a 50% probability level.

Table S2. Selected crystal data and structure refinement data of [Cu(**R6**)](PF_6).

Moiety formula	$C_{118}H_{141}CuF_6N_5O_7P$
Formula weight	1947.98
Crystal system	Monoclinic
Space group	$P2_1/n$
Color of crystal	Orange
Temperature/K	100
a/Å	34.636(7)
b/Å	16.348(3)
c/Å	20.073(4)
α/°	90
β/°	92.404(5)
γ/°	90
Volume/Å^3	11356(4)
Z	4
$\rho_{\chi\alpha\lambda\chi}$/gcm^3	1.213
μ/mm^{-1}	0.275
F(000)	4416.0
Crystal size/mm^3	0.04 × 0.02 × 0.02
Radiation/Å	MoKα (λ = 0.71073)
$\theta_{\mu\nu}$, $\theta_{\mu\alpha\xi}$/°	2.756, 48.998
Index ranges	-40 ≤h≤ 40, 0 ≤k≤19, 0 ≤l≤ 23
Data/restraints/parameters	18427/11/1322
Final R indexes [I≥2σ(I)]	R_1 = 0.1500, wR_2 = 0.3039
Final R indexes [all data]	R_1 = 0.1847, wR_2 = 0.3263
Largest diff. peak/hole / e Å^{-3}	0.97/-1.03
Restrained goodness of fit	1.223

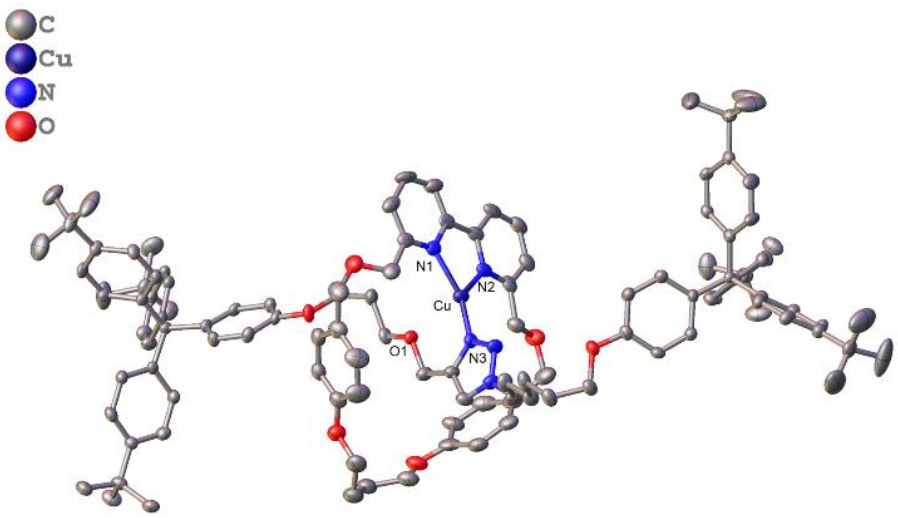

Fig. S31. Crystal structure of [Cu(**R4**)](PF$_6$) (CCDC: 2504020). All H atoms have been omitted for clarity. Thermal ellipsoids are scaled to a 50% probability level.

Table S3. Selected crystal data and structure refinement data of [Cu(**R4**)](PF$_6$).

Moiety formula	$C_{116}H_{137}CuF_6N_5O_7P$
Formula weight	1919.95
Crystal system	Triclinic
Space group	P-1
Color of crystal	Orange
Temperature/K	100
a/Å	14.1927(10)
b/Å	16.1321(10)
c/Å	27.927(2)
α/°	90.618(5)
β/°	104.435(5)
γ/°	108.908(4)
Volume/Å^3	5828.9(7)
Z	2
$\rho_{\chi\alpha\lambda\chi}$/gcm^3	1.203

μ/mm^{-1}	0.945
F(000)	2256.0
Crystal size/mm^3	0.1 × 0.05 × 0.03
Radiation/Å	CuKα (λ = 1.54178)
$\theta_{\mu\iota\nu}$, $\theta_{\mu\alpha\xi}$/°	3.284, 118.684
Index ranges	-15 ≤ h ≤ 15, -17 ≤ k ≤ 17, -31 ≤ l ≤ 31
Data/restraints/parameters	16816/105/1365
Final R indexes [I≥2σ(*I*)]	R_1 = 0.0767, wR_2 = 0.1886
Final R indexes [all data]	*R_1 = 0.1262, wR_2 = 0.2189*
Largest diff. peak/hole / e Å^{-3}	1.18/-0.64
Restrained goodness of fit	1.024

2. Electrochemical Measurements.

2.1 General Methods.

Chemicals for synthesis were obtained from commercial sources and used as received unless otherwise stated. Electrochemical studies at pH 4 and pH 7 were performed in Britton–Robinson buffer (BR) containing H_3BO_3 (0.04 M, 99.999%, Fisher Scientific), CH_3COOH (0.04 M, 100%, VWR), H_3PO_4 (0.04 M, 85 wt % in H_2O, J&K Scientific), $NaClO_4$ (0.1 M, 99.9%, Sigma-Aldrich) and Milli-Q ultrapure water (>18.2 MΩ cm). Solutions were adjusted to pH 4 and pH 7 respectively using NaOH (10 M, analytical grade, Merck Millipore), and subjected to 30-min sparging with either N_2 or O_2 (99.995% high-purity grade, Linde HKO) before electrochemical measurements.

2.2 Catalyst Ink Preparations.

Multiwalled carbon nanotubes were pretreated by immersing in 6 M HCl (Duksan, 37% GR) for 24 hours. The acid-treated carbon nanotubes were subsequently filtered, rinsed with Milli-Q ultrapure water, and dried overnight in a vacuum oven at 80 °C. The Cu catalyst (2.0 mg) was dissolved in CH_3CN (RCI Labscan, AR) and mixed with the acid-treated carbon nanotubes (8.0 mg) to form a catalyst/carbon mixture. The mixture was sonicated for 5 min and subsequently vacuum-dried at 37 °C overnight. The catalyst/carbon mixture (4.0 mg) was finely ground and then suspended in absolute CH_3OH (1.0 mL, Scharlab, Abs) and sonicated for 15 min. Nafion

perfluorinated resin (10 μL, 5 wt% in lower aliphatic alcohols with 15−20% water, Sigma-Aldrich) was added to the well-dispersed catalyst ink. The catalyst ink was sonicated for an additional 10 min and was drop-casted (15.0 μL) onto a polished glassy carbon disk electrode (A = 0.196 cm^2). The electrode was then dried under a stream of N_2.

2.3 Electrochemical Activity Measurements.

The electrocatalytic oxygen reduction activity was evaluated in a three-electrode electrochemical cell. A polished glassy carbon (GC) electrode served as the working electrode, a graphite rod as the counter electrode, and an aqueous "no-leak" Ag/AgCl (3 M KCl, EDAQ Inc) as the reference electrode. At both pH 4 and pH 7, ORR onset potential is defined as the potential at which 10 μA/cm^2 current density is reached. The $Cu^{II/I}$ redox properties of Cu^I rotaxanes were characterised in 0.1 M tetrabutylammonium hexafluorophosphate (NBu_4PF_6) in CH_3CN, using GC as the working electrode and a graphite rod as the counter electrode, with an Ag wire immersed in 10 mM $AgNO_3$ (in CH_3CN) as a pseudo-reference. The $Cu^{II/I}$ redox couples were referenced against 1 mM ferrocene (Fc/Fc^+) in NBu_4PF_6 in CH_3CN. Cyclic voltammetry (CV) and linear sweep voltammetry (LSV) experiments were conducted using a CH Instruments 660E potentiostat at a scan rate of 10 mV/s for ORR activity measurement and 100 mV/s for $Cu^{II/I}$ and Fc/Fc^+ redox measurements. All experiments were performed in triplicates, and error bars represent the standard deviations of the triplicate trials. The GC electrode was polished using a 3 to 0.5 μm alumina suspension polishing kit (Allied Tech) and cleaned by electrochemical cycling from -0.4 to 1.7 V vs. Ag/AgCl in 0.1 M $HClO_4$. Electrochemical potentials were referenced to the reversible hydrogen electrode (RHE) according to established protocols.[5,6]

2.4 Product Quantification.

The electrocatalytic oxygen reduction selectivity was assessed through a colorimetric assay for H_2O_2 quantification, following a previously reported protocol.[7,8] Briefly, the concentration of H_2O_2 was determined using cerium(IV) sulfate ($Ce(SO_4)_2$) titration at pH 4 and Amplex Red assay at pH 7. A solution of $Ce(SO_4)_2$ (1.0 mM) was prepared by dissolving $Ce(SO_4)_2 \cdot 4H_2O$ (4.0 mg) in 0.5 M H_2SO_4 (10.0 mL). A standard curve for H_2O_2 was generated by adding the prepared cerium titrant (0.1 mL) to H_2O_2 solutions (0.9 mL) with known concentrations (0.5, 1.0, 2.0, 5.0, 10.0 μM). A working solution of Amplex Red was prepared by mixing of 10 mM Amplex Red (40 μL) in DMSO with of 0.05 M pH 7 sodium phosphate buffer (3.88 mL) containing of 10 U/mL

horseradish peroxidase (HRP) (80 μL). A standard curve for H_2O_2 was generated by adding the prepared Amplex Red (0.5 mL) to H_2O_2 solutions (0.5 mL) with known concentrations (1.0, 2.5, 5.0, 10.0 μM). The absorbance at 316 nm ($Ce(SO_4)_2$ titration) and 571 nm (Amplex Red assay) were recorded respectively to determine the H_2O_2 concentration based on the calibration curve.

2.5 Calculations of H_2O Selectivity.

The number of electrons transferred per O_2 molecule (*n*) during oxygen reduction reaction by the Cu^I rotaxane complexes was determined following a reported method,[9,10] where *x* represents the mole fraction of O_2 consumed for H_2O_2 generation, relative to total O_2 consumed for H_2O_2 and H_2O generation.

$$n = 4(1 - x) + 2x$$

$$x = \frac{mole\ of\ O_2\ reduced\ (H_2O_2)}{total\ mole\ of\ O_2\ reduced\ (H_2O_2 + H_2O)}$$

$$\%\ H_2O = \frac{n - 2}{2} \times 100\ \%$$

2.6 Metal Quantifications.

The quantity of Cu in catalyst-loaded was determined using inductively coupled plasma mass spectrometry (ICP-MS) (Agilent 7700x). The catalyst ink (10 μL) was added in aqua regia (9.99 mL, 1:3 *v*/*v* HNO_3:HCl) and left standing for 24 h. The resulting catalyst/acid mixture was filtered using a PES syringe filter (Labfil, 0.22 μm). The filtrate (490 μL) and an internal standard (10000 ppb Rh, 10 μL) were added to 1% HNO_3 (9.5 mL).

2.7 Experimental Results.

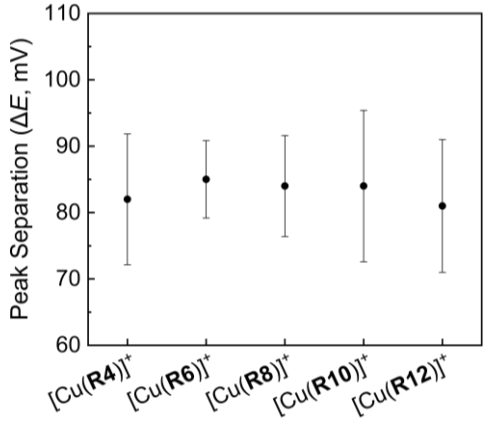

Fig. S32. $Cu^{II/I}$ redox characterisation of Cu^{I} rotaxanes. Peak separation (ΔE) of the $Cu^{II/I}$ redox couple in 0.1 M NBu_4PF_6 in CH_3CN. Error bars represent the standard deviations of the triplicate trials.

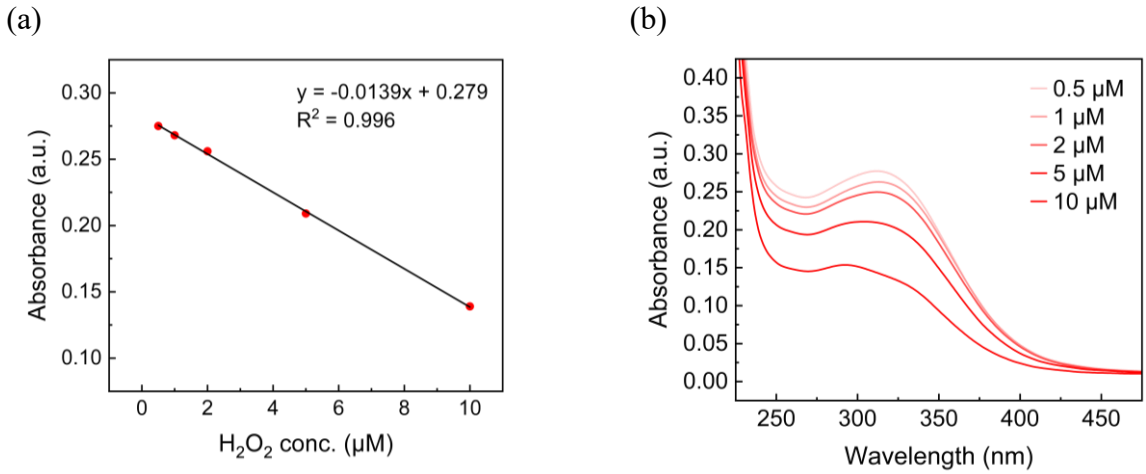

Fig. S33. H_2O_2 colorimetric assay using $Ce(SO_4)_2$ titration method. (a) Standard curve of H_2O_2 with known concentrations. (b) UV-vis absorption spectra of the H_2O_2 standards.

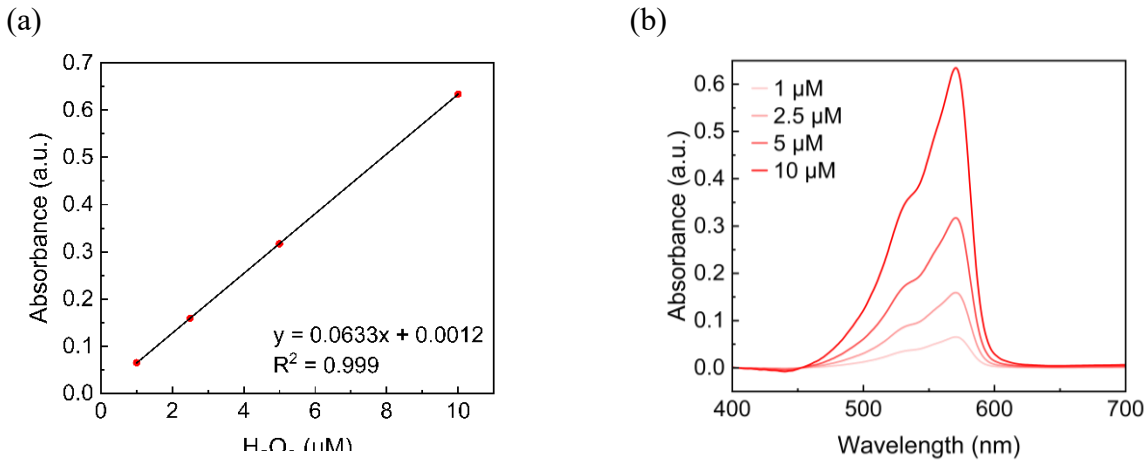

Fig. S34. H_2O_2 colorimetric assay using Amplex Red assay. (a) Standard curve of H_2O_2 with known concentrations. (b) UV-vis absorption spectra of the H_2O_2 standards.

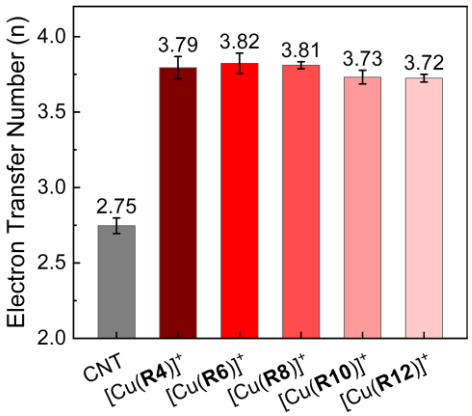

Fig. S35. Electron transfer number (n) of ORR catalysed by carbon nanotubes (CNT), [Cu(**R4**)]$^+$, [Cu(**R6**)]$^+$, [Cu(**R8**)]$^+$, [Cu(**R10**)]$^+$, and [Cu(**R12**)]$^+$ supported on glassy carbon electrode (GC) in pH 4 BR buffer. Error bars represent the standard deviations of the triplicate trials.

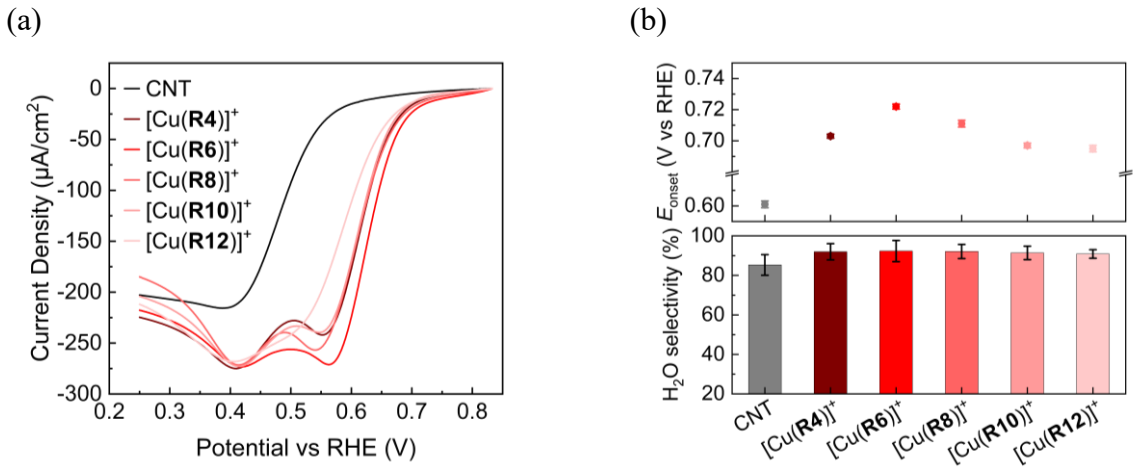

Fig. S36. (a) Linear sweep voltammograms of carbon nanotubes (CNT), [Cu(**R4**)]$^+$, [Cu(**R6**)]$^+$, [Cu(**R8**)]$^+$, [Cu(**R10**)]$^+$, and [Cu(**R12**)]$^+$ supported on glassy carbon electrode (GC) in O_2-saturated pH 7 BR buffer, and (b) their respective ORR onset potential and product selectivity. The ORR onset potential is defined as the potential at which 10 μA/cm^2 is reached. Error bars represent the standard deviations of the triplicate trials.

At both pH 4 and pH 7, a second ORR reduction peak was observed in the LSV curves for all Cu^I rotaxanes, occurring at *c.a.* 0.25 V (vs. RHE) and *c.a.* 0.40 V (vs. RHE), respectively (Fig. 4, S36). This peak is attributed to the background ORR activity of the CNT support.

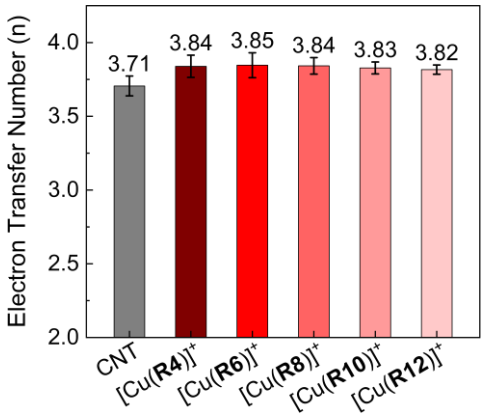

Fig. S37. Electron transfer number (n) of ORR catalysed by carbon nanotubes (CNT), [Cu(**R4**)]$^+$, [Cu(**R6**)]$^+$, [Cu(**R8**)]$^+$, [Cu(**R10**)]$^+$, and [Cu(**R12**)]$^+$ supported on glassy carbon electrode (GC) in pH 7 BR buffer. Error bars represent the standard deviations of the triplicate trials.

Table S4. ORR onset potentials and electron transfer number of reported molecular Cu catalysts.

Molecular Cu complexes	**Onset potential (V vs RHE)**		**Electron transfer number (n)**		**References**
	pH 4	pH 7	pH 4	pH 7	
[Cu(**R6**)]$^{+}$	0.58	0.72	3.8	3.9	This work
[Cu(2-(5-(pyren-1-yl) pentyl)-9-methyl-1,10-phenanthroline)$_2$]$^{2+}$	0.86 (pH 5)	-	3.9 (pH 5)	-	[11]
[Cu(2,9-Me$_2$-phen)$_2$]$^{+}$	0.72 (pH 5.2)	-	2.7 (pH 5.2)	-	[12]
[Cu(2,9-Me$_2$-4,7-Ph$_2$-phen)$_2$]$^{+}$	0.69 (pH 5.2)	-	2.9 (pH 5.2)	-	[12]
[Cu(3,8-Br$_2$-phen)$_2$]$^{+}$	0.61 (pH 5.2)	-	3.8 (pH 5.2)	-	[12]
[Cu(LH)]$^{2+}$	0.60 (pH 5)	-	3.3 (pH 5)	-	[13]
[Cu(5-Cl-phen)$_2$]$^{+}$	0.60 (pH 5.2)	-	3.1 (pH 5.2)	-	[12]
Au|Cu(DAT)	*ca.* 0.6 (pH 5.2)	-	-	-	[14]
[Cu(phen)$_2$]$^{+}$	0.58 (pH 5.2)	-	3.1 (pH 5.2)	-	[12]
[Cu(2,9-Et$_2$-phen)]$^{2+}$	0.59 (pH 4.8)	-	-	-	[15,16]
[Cu(TPA)]$^{2+}$	0.57	0.69	3.6		[5]
[Cu$_2$(BPMP-pyrene)]$^{2+}$	0.57	-	2.7	-	[17]
[Cu(PMAP)]$^{2+}$	0.57	-	2.5	-	[5]
[Cu(4,7-Me$_2$-phen)$_2$]$^{+}$	0.56 (pH 5.2)	-	3.7 (pH 5.2)	-	[12]
[Cu(3,4,7,8-Me$_4$-phen)$_2$]$^{+}$	0.55 (pH 5.2)	-	3.8 (pH 5.2)	-	[12]
[Cu(2,9-nBu$_2$-phen)]$^{2+}$	0.55 (pH 4.8)	-	-	-	[15,16]
Cu(phen^{C})	0.53 (pH 4.8)	-	3.6 (pH 4.8)	-	[18]

$[Cu(TPT)]^{2+}$	0.51 (pH 5.3)	-	1.9	-	[19]
$[Cu(5\text{-}Cl\text{-}phen)]^{2+}$	0.49 (pH 5.2)	-	*ca.* 3.5	-	[20]
$[Cu(TPP)]^{2+}$	0.44	-	-	-	[21]
$[Cu(2\text{-}Cl\text{-}phen)_2]^{+}$	0.42 (pH 5.2)	-	2.8 (pH 5.2)	-	[12]
$[Cu(4,7\text{-}dppds)]^{2+}$	0.41 (pH 5.3)	-	-	-	[22]
PG|Cu(DAT)	*ca.* 0.4 (pH 5.2)	--	1.2 (pH 5.2)	-	[14]
[Cu(phen)]/Au	0.40	-	-	-	[23]
$[Cu(3\text{-}ethynyl\text{-}phen)]^{+}$	0.39 (pH 4.8)	-	3.6	-	[18]
$[Cu(phen)]^{2+}$	0.30 (pH 4.8)	-	-	-	[24]
MWCNT@BTAH-Cu^{2+}	-	0.74	-	*ca.* 3.8	[25]
$Cu(ImBenz\text{-}NO_2)Cl_2$	-	0.69	-	3.5–3.8	[26]
$[Cu(C10)]^{+}$	-	0.62	-	*ca.* 3.8	[6]
$[Cu(3,5\text{-}dimethyl\text{-}4\text{-}amino\text{-}1,2,4\text{-}triazole)]^{2+}$	-	0.58	-	-	[16]
$[Cu(trpn)(Im)]^{2+}$	-	0.58	-	-	[27]
$[Cu(baEtO)(Im)]^{2+}$	-	0.57	-	-	[28]
Cu^{2+}:L_2	-	0.55	-	3.2–3.8	[29]
$[Cu(dpaq)]^{+}$	-	0.50	-	3.8	[30]
CuPoly-CB	-	0.50	-	2.7	[31]
$[Cu(bmpa)]^{2+}$	-	0.49	-	*ca.* 2.5–2.7	[32]
Cu-tpmen	-	0.47	-	*ca.* 2.3-3.2	[33]
Cu-tpbn-Me_2bpy	-	0.46	-	2.9–3.4	[34]

$[Cu(terpy)]^{2+}$	-	0.45	-	*ca.* 2.5–2.7	[32]

LH = (2-tert-butyl-6-{[(6-methyl-pyridin-2-ylmethyl)-pyridin-2-ylmethyl-amino]-methyl}-4-({4-[(pyren-1-ylmethyl)-amino]-butylamino}-methyl)-phenol), Au| = modified gold electrode; DAT = 3,5-diamino-1,2,4-triazole, TPA = tris(2-pyridylmethyl)amine, BPMP = 2,6-bis[(bis(2-pyridylmethyl)amino)methyl]-phenol, PMAP = bis[2-(2-pyridyl)ethyl]-(2-pyridyl)methylamine, phen^{c} = 3-ethynyl-1,10-phenanthroline was covalently attached to an azide-modified glassy carbon electrode by cycloaddition, TPT = 2,4,6-tris(2-piridil)-1,3,5-triazine, TPP = 5,10,15,20-tetraphenyl-21H,23H-porphyrin, dppds = 4,7-diphenyl-1,10-phenanthrolinedisulfonate, PG| = modified pyrolytic graphite electrode, BTAH = 1,2,3-benzotriazole, ImBenz-NO_2 = 2-(1-(2,6-diisopropylphenyl)-1H-imidazol-2-yl)-5-nitro-1H-benzo[d]imidazole], C10 = [2]catenane derivatives, trpn = tris(3-aminopropyl)amine, baEtO = 2-[bis(2-aminoethyl)amino]ethanol, L_2 = ligand obtained from polymerizations of poly(ethylene glycol) diglycidyl ether (PEGDGE) and 2,2′-bipyridine-5,5′-dicarboxylic acid, dpaq = 2-[bis(pyridine-2-ylmethyl)]amino-N-quinolin-8-yl-acetamidate, Poly, = pyrene-terminated poly(2-hydroxy-3-dipicolylamino) propyl methacrylate (Py-PGMADPA); CB = carbon black, bmpa = bis(2-pyridylmethyl)amine, tpbn = tetrapyridylalkylamine N,N,N’,N’-tetrakis(2-pyridyl-methyl)-1,4-butanediamine, terpy = 2,2′:6′,2″-terpyridine, tpmen = N,N,N’-tris(2-pyridylmethyl)-N’-methylethylenediamine.

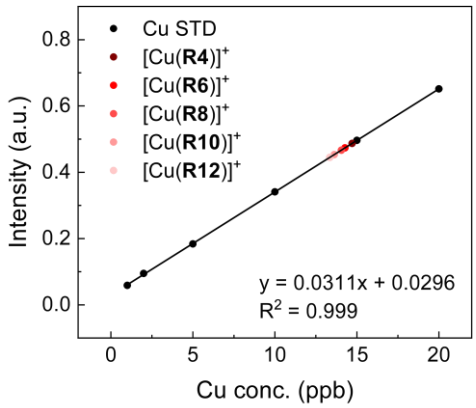

Fig. S38. ICP-MS results of Cu^{I} rotaxane complexes.

Table S5. Concentration of Cu metal in rotaxane complexes.

Samples	**Cu/Rh ratio**	**Cu conc. (μmol/cm^2)**
[Cu(**R4**)]$^+$	0.487	0.0236
[Cu(**R6**)]$^+$	0.473	0.0229
[Cu(**R8**)]$^+$	0.467	0.0226
[Cu(**R10**)]$^+$	0.453	0.0219
[Cu(**R12**)]$^+$	0.445	0.0214

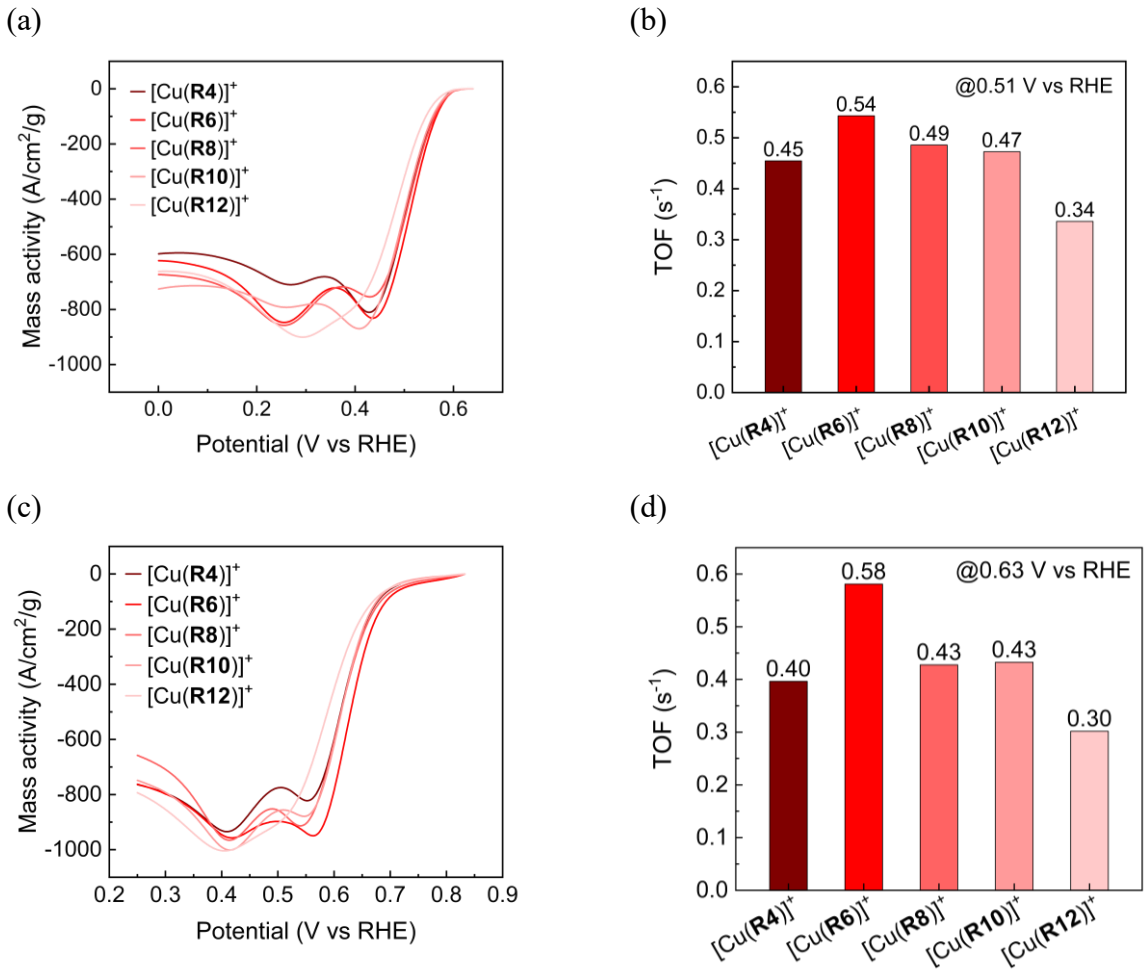

Fig. S39. Mass activity and turnover frequency (TOF) of [Cu(**R4**)]$^+$, [Cu(**R6**)]$^+$, [Cu(**R8**)]$^+$, [Cu(**R10**)]$^+$, and [Cu(**R12**)]$^+$ with their ORR current densities normalized by Cu quantity in (a, b) pH 4 BR buffer and (c, d) pH 7 BR buffer.

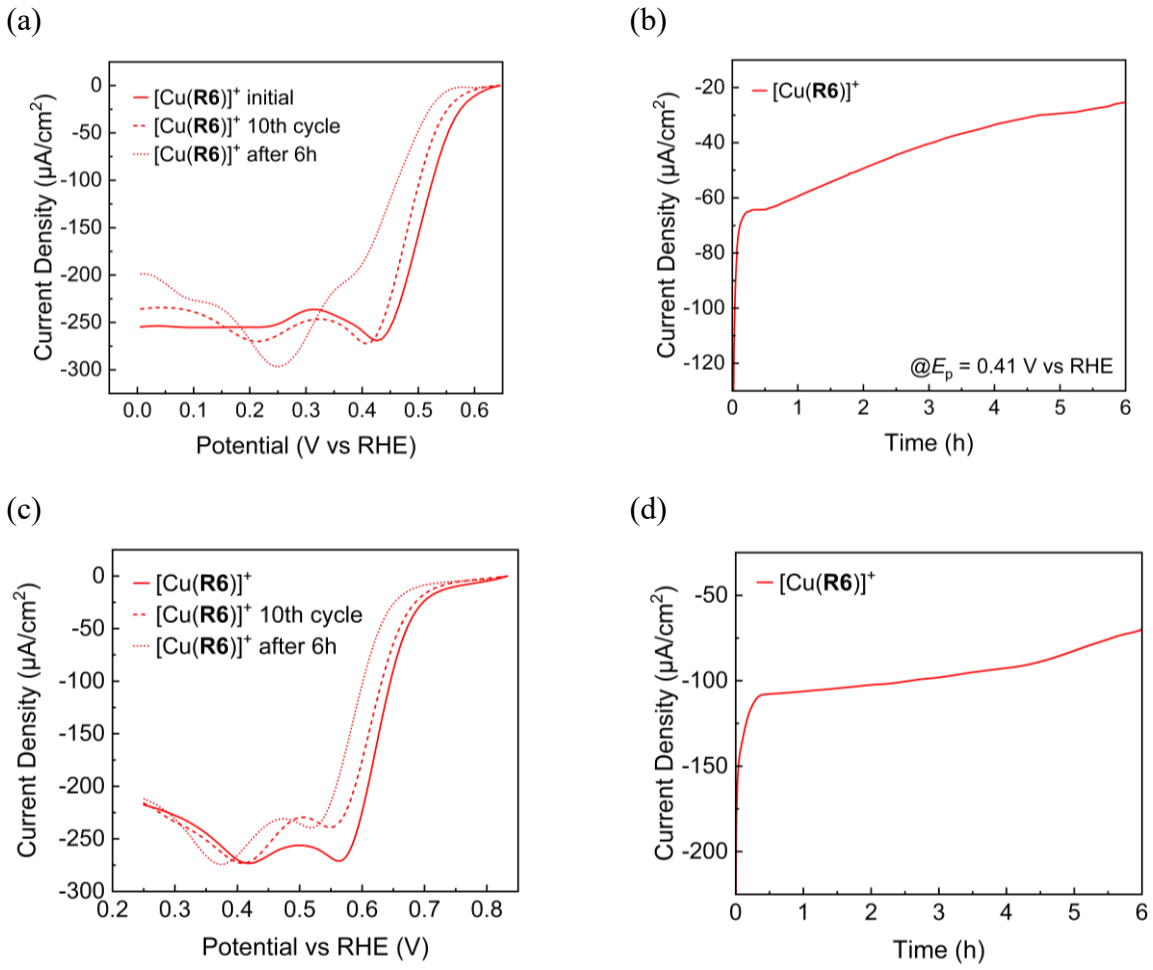

Fig. S40. Linear sweep voltammograms (LSV) of [Cu(**R6**)]$^+$ at the initial stage (solid red), at 10th consecutive LSV scan (dashed red), and after 6 hours of chronoamperometry test (dotted red). Chronoamperometry curve of [Cu(**R6**)]$^+$ recorded over 6 hours at E_p. Data in (a) and (b) were collected in pH 4 BR buffer, while data in (c) and (d) were recorded in pH 7 BR buffer.

(a)

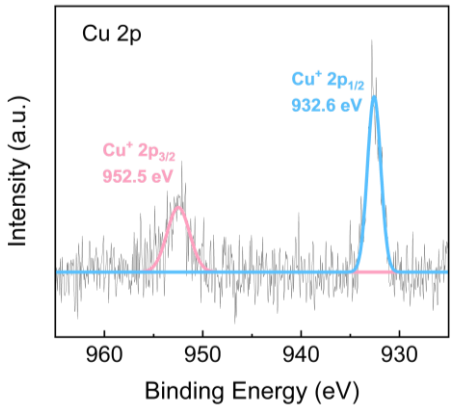
Cu 2p
Cu+ 2p1/2
932.6 eV
Cu+ 2p3/2
952.5 eV
Intensity (a.u.)
960
950
940
930
Binding Energy (eV)

(b)

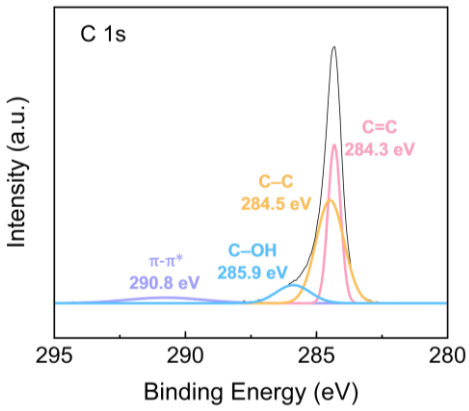
C 1s
C=C
284.3 eV
C–C
284.5 eV
C–OH
285.9 eV
π-π*
290.8 eV
Intensity (a.u.)
295
290
285
280
Binding Energy (eV)

(c)

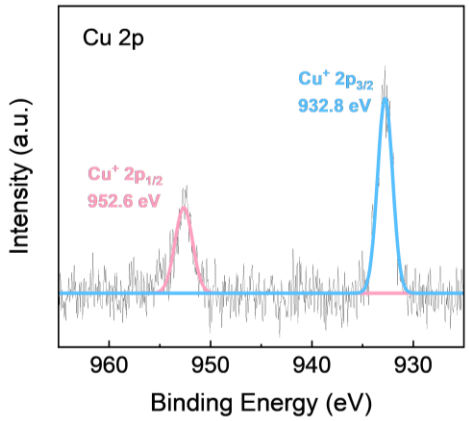
Cu 2p
Cu+ 2p3/2
932.8 eV
Cu+ 2p1/2
952.6 eV
Intensity (a.u.)
960
950
940
930
Binding Energy (eV)

(d)

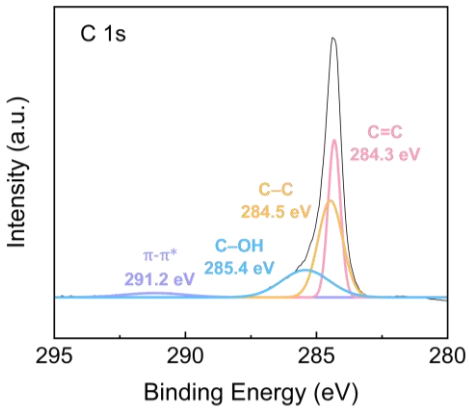
C 1s
C=C
284.3 eV
C–C
284.5 eV
C–OH
285.4 eV
π-π*
291.2 eV
Intensity (a.u.)
295
290
285
280
Binding Energy (eV)

(e)

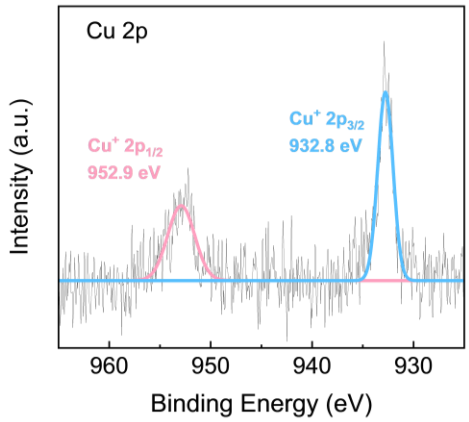
Cu 2p
Cu+ 2p3/2
932.8 eV
Cu+ 2p1/2
952.9 eV
Intensity (a.u.)
960
950
940
930
Binding Energy (eV)

(f)

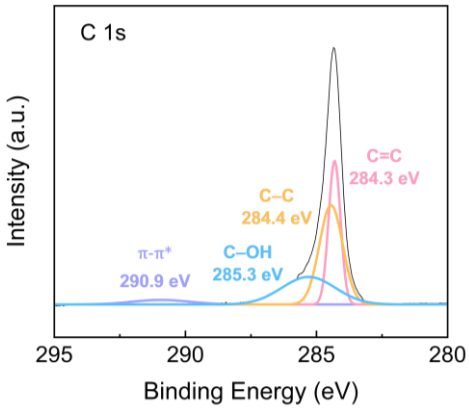
C 1s
C=C
284.3 eV
C–C
284.4 eV
C–OH
285.3 eV
π-π*
290.9 eV
Intensity (a.u.)
295
290
285
280
Binding Energy (eV)

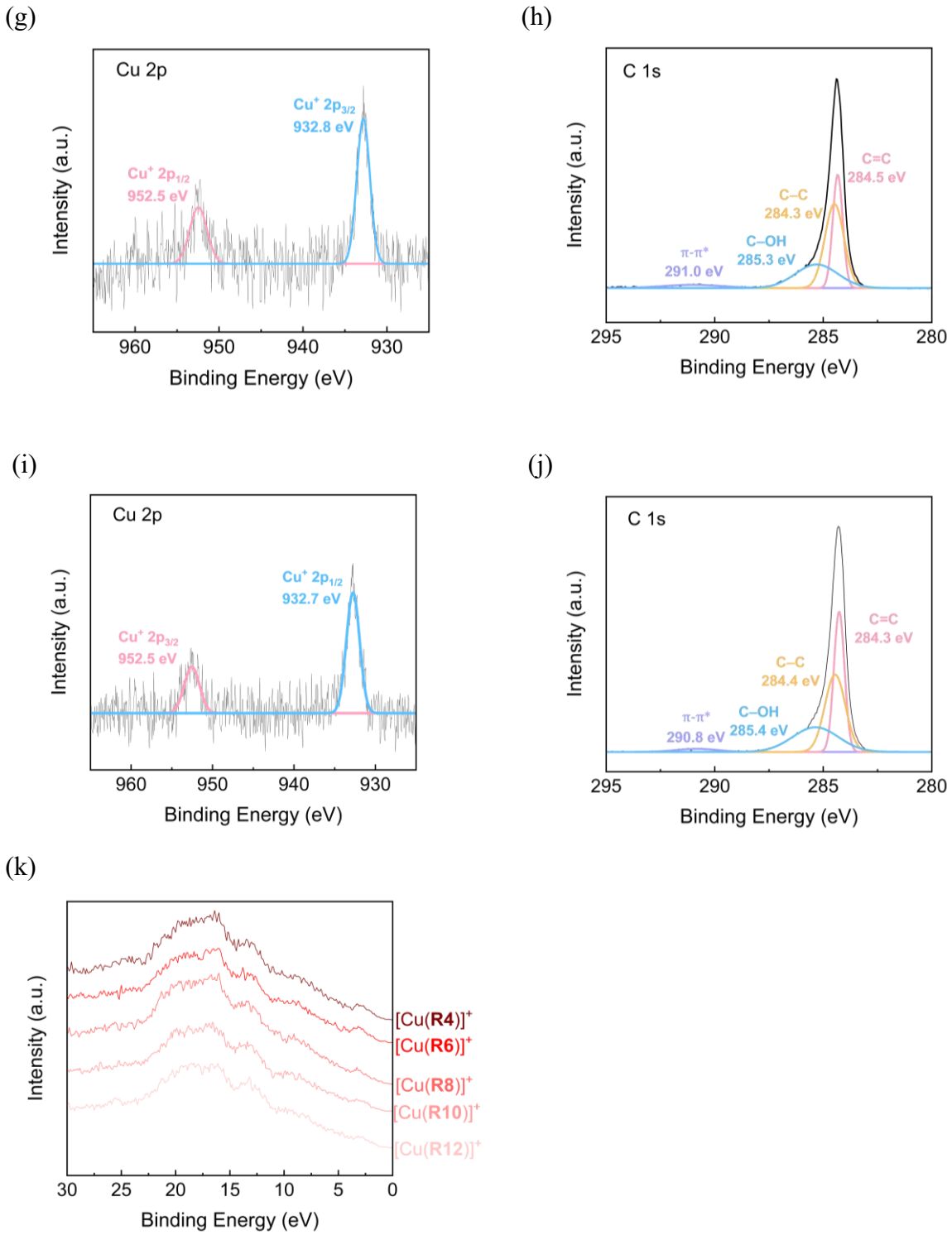

Fig. S41. High-resolution X-ray photoelectron (XPS) spectra of Cu 2p, C 1s, and (k) valence band for (a,b) [Cu(**R4**)]$^+$, (c,d) [Cu(**R6**)]$^+$, (e,f) [Cu(**R8**)]$^+$, (g,h) [Cu(**R10**)]$^+$, and (i,j) [Cu(**R12**)]$^+$ before ORR.

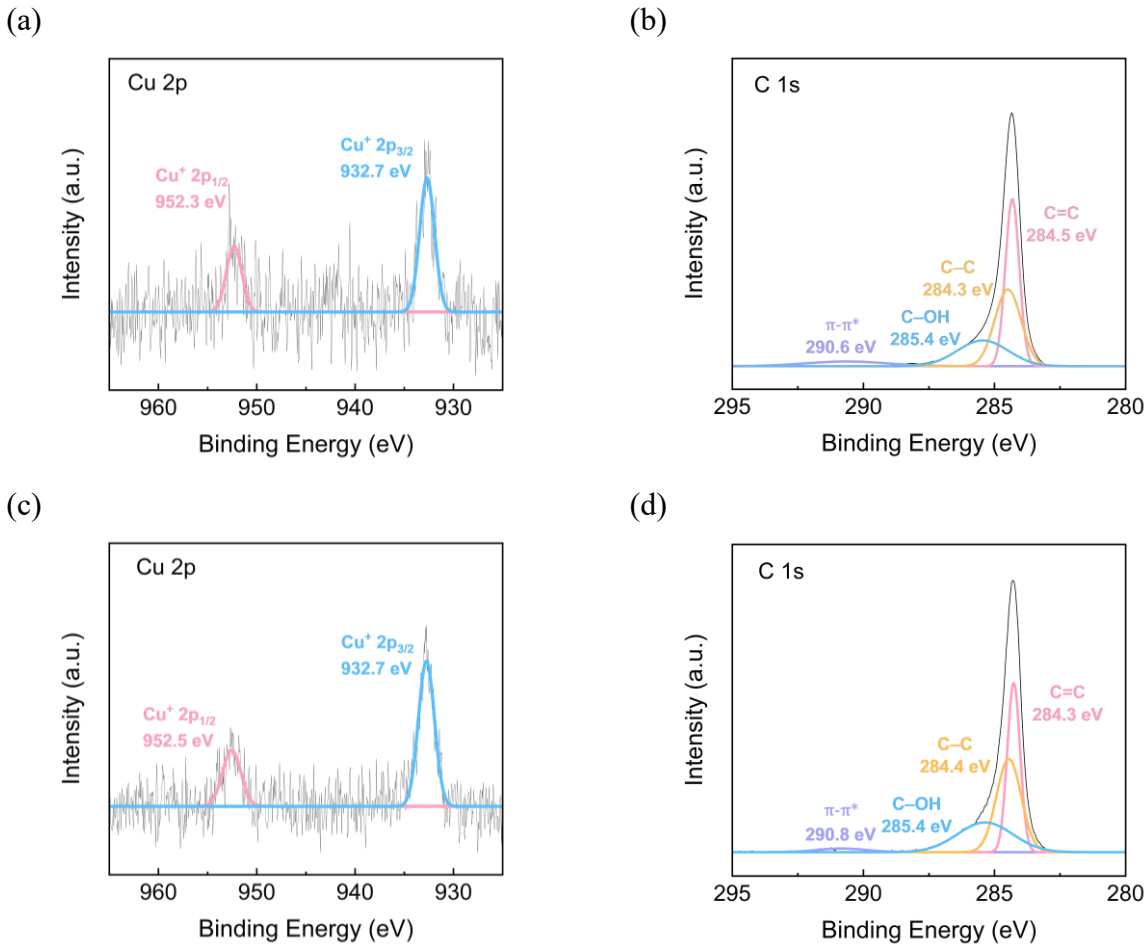

Fig. S42. High-resolution XPS spectra of Cu 2p and C 1s for $[Cu(\mathbf{R6})]^{+}$ after 10 consecutive ORR LSV scans (a,b) at pH 4 and (c, d) at pH 7.

(a)

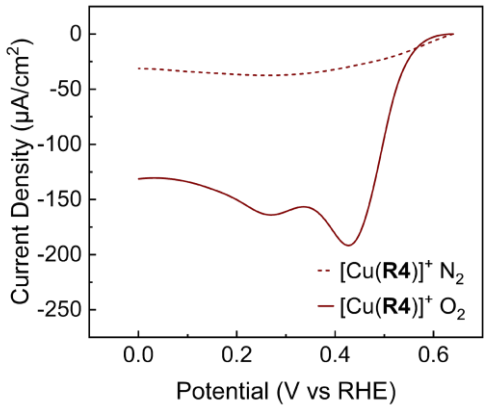
Current Density (μA/cm²)
0
-50
-100
-150
-200
-250
0.0
0.2
0.4
0.6
Potential (V vs RHE)
[Cu(R4)]⁺ N₂
[Cu(R4)]⁺ O₂

(b)

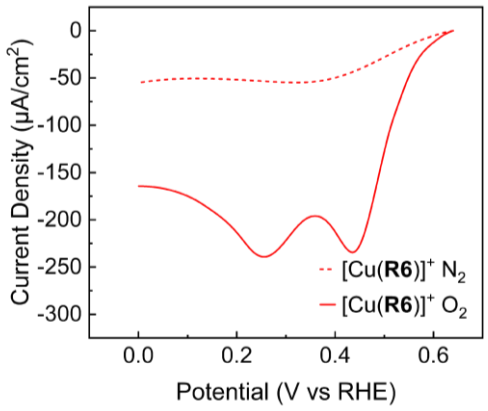
Current Density (μA/cm²)
0
-50
-100
-150
-200
-250
-300
0.0
0.2
0.4
0.6
Potential (V vs RHE)
[Cu(R6)]⁺ N₂
[Cu(R6)]⁺ O₂

(c)

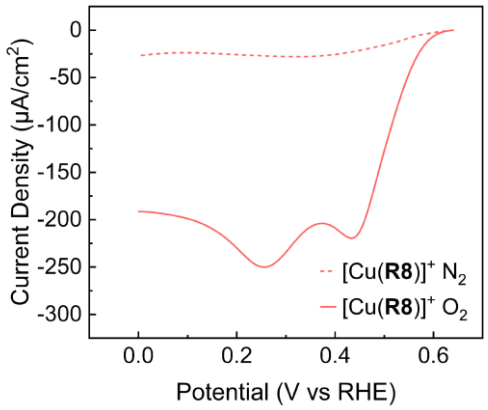
Current Density (μA/cm²)
0
-50
-100
-150
-200
-250
-300
0.0
0.2
0.4
0.6
Potential (V vs RHE)
[Cu(R8)]⁺ N₂
[Cu(R8)]⁺ O₂

(f)

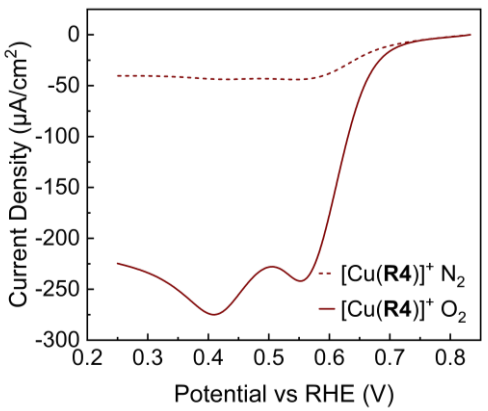
Current Density (μA/cm²)
0
-50
-100
-150
-200
-250
-300
0.2
0.3
0.4
0.5
0.6
0.7
0.8
Potential vs RHE (V)
[Cu(R4)]⁺ N₂
[Cu(R4)]⁺ O₂

(g)

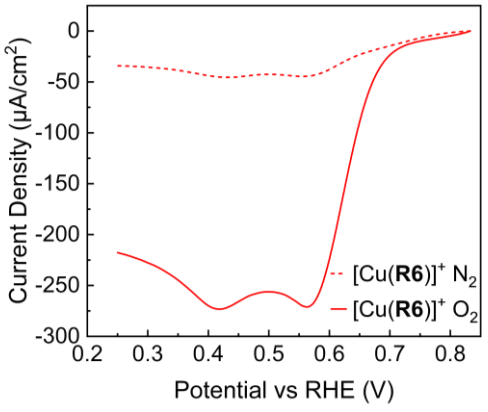
Current Density (μA/cm²)
0
-50
-100
-150
-200
-250
-300
0.2
0.3
0.4
0.5
0.6
0.7
0.8
Potential vs RHE (V)
[Cu(R6)]⁺ N₂
[Cu(R6)]⁺ O₂

(h)

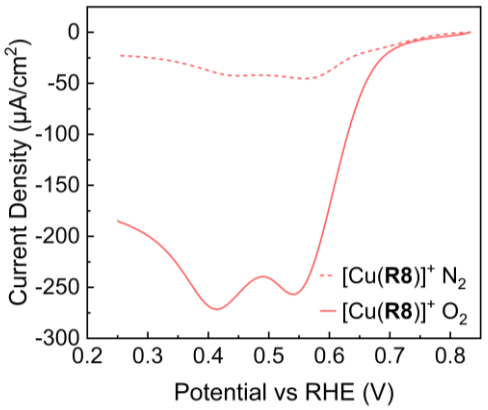
Current Density (μA/cm²)
0
-50
-100
-150
-200
-250
-300
0.2
0.3
0.4
0.5
0.6
0.7
0.8
Potential vs RHE (V)
[Cu(R8)]⁺ N₂
[Cu(R8)]⁺ O₂

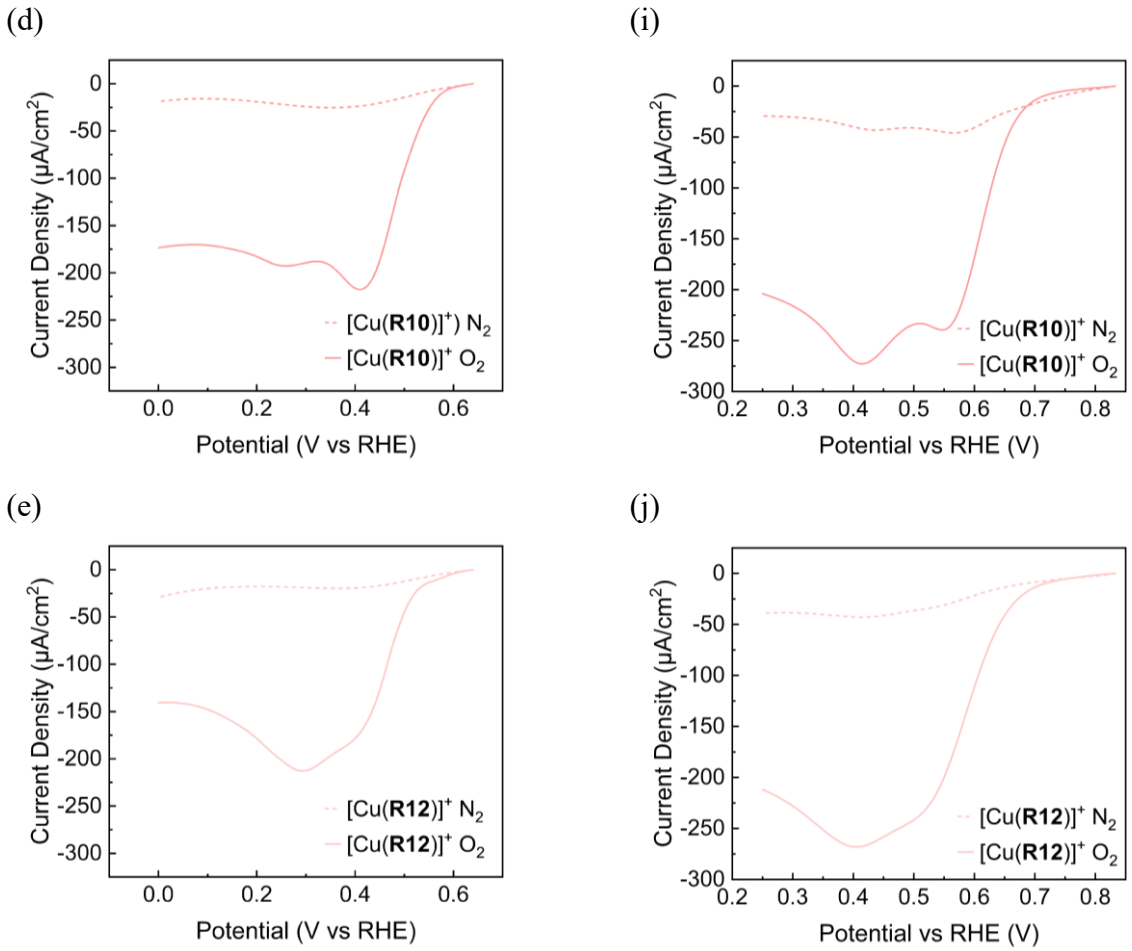

Fig. S43. Cyclic voltammograms of all Cu^{I} rotaxane complexes under N_2-saturated (dotted) and O_2-saturated (solid) electrolytes in BR buffers at (a-e) pH 4 and (f-j) pH 7.

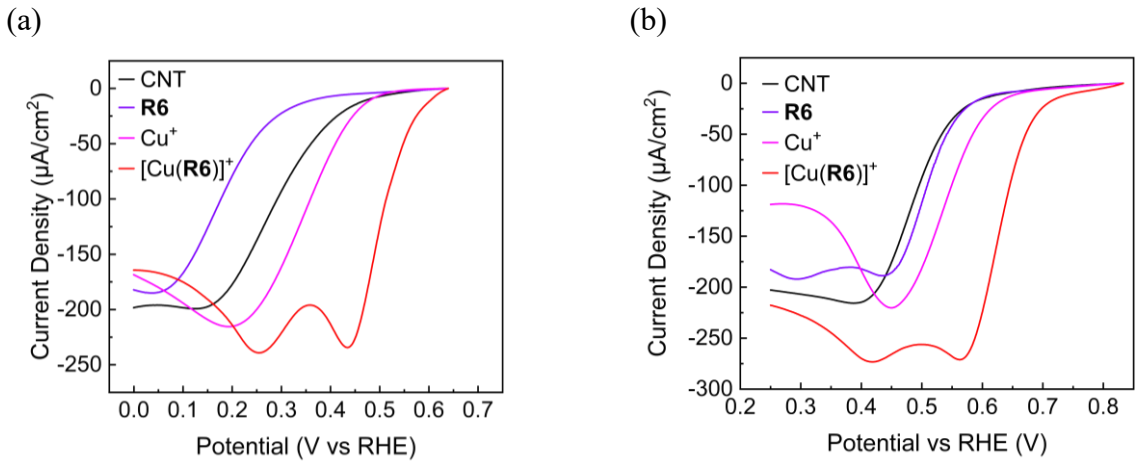

Fig. S44. Linear sweep voltammograms of ORR catalysed by heterogenous **R6** and [Cu(**R6**)]$^{+}$ supported on carbon nanotubes (CNT), homogenous Cu^{+} ions (2 mM $[Cu(MeCN)_4](PF_6)$), and CNT only in BR buffer at (a) pH 4 and (b) pH 7.

Supporting References

1. J. D. Crowley, K. D. Hänni, A.-L. Lee and D. A. Leigh, *J. Am. Chem. Soc.*, 2007, **129**, 12092–12093.

2. J. E. M. Lewis, R. J. Bordoli, M. Denis, C. J. Fletcher, M. Galli, E. A. Neal, E. M. Rochette and S. M. Goldup, *Chem. Sci.*, 2016, **7**, 3154–3161.

3. A. Al Abbas, B. Heinrich, M. L'Her, E. Couzigné, R. Welter and L. Douce, *New J. Chem.*, 2017, **41**, 2604–2613.

4. O. V. Dolomanov, L. J. Bourhis, R. J. Gildea, J. A. K. Howard and H. Puschmann, *J. Appl. Cryst.*, 2009, **42**, 339–341.

5. M. A. Thorseth, C. S. Letko, E. C. M. Tse, T. B. Rauchfuss and A. A. Gewirth, *Inorg. Chem.*, 2013, **52**, 628–634.

6. X. Mo, Y. Deng, S. K.-M. Lai, X. Gao, H.-L. Yu, K.-H. Low, Z. Guo, H.-L. Wu, H. Y. Au-Yeung and E. C. M. Tse, *J. Am. Chem. Soc.*, 2023, **145**, 6087–6099.

7. Z. Lu, G. Chen, S. Siahrostami, Z. Chen, K. Liu, J. Xie, L. Liao, T. Wu, D. Lin, Y. Liu, T. F. Jaramillo, J. K. Nørskov and Y. Cui, *Nat. Catal.*, 2018, **1**, 156–162.

8. W. Zhou, X. Mo, C. W. Cheung and E. C. M. Tse, *J. Chem. Eng.*, 2024, **500**, 157129.

9. E. C. M. Tse, C. J. Barile, N. A. Kirchschlager, Y. Li, J. P. Gewargis, S. C. Zimmerman, A. Hosseini and A. A. Gewirth, *Nat. Mater.*, 2016, **15**, 754–759.

10. T. Zeng, J. Chen, Z. H. Yu and E. C. M. Tse, *J. Am. Chem. Soc.*, 2024, **146**, 31757–31767.

11. D. Brazzolotto, Y. Nedellec, C. Philouze, M. Holzinger, F. Thomas and A. Le Goff, *Inorg. Chem.*, 2022, **61**, 14997–15006.

12. R. Venegas, K. Muñoz-Becerra, L. Lemus, A. Toro-Labbé, J. H. Zagal and F. J. Recio, *J. Phys. Chem. C*, 2019, **123**, 19468–19478.

13. S. Gentil, D. Serre, C. Philouze, M. Holzinger, F. Thomas and A. Le Goff, *Angew. Chem. Int. Ed. Engl.*, 2016, **55**, 2517–2520.

14. B. van Dijk, J. P. Hofmann and D. G. H. Hetterscheid, *Phys. Chem. Chem. Phys.*, 2018, **20**, 19625−19634.

15. C. C. McCrory, X. Ottenwaelder, T. D. Stack and C. E. Chidsey, *J. Phys. Chem. A*, 2007, **111**, 12641–12650.

16. M. A. Thorseth, C. E. Tornow, E. C. M. Tse and A. A. Gewirth, *Coord. Chem. Rev.*, 2013, **257**, 130–139.

17. S. Gentil, J. K. Molloy, M. Carrière, A. Hobballah, A. Dutta, S. Cosnier, W. J. Shaw, G. Gellon, C. Belle, V. Artero, F. Thomas and A. Le Goff, *Joule*, 2019, **3**, 2020–2029.

18. C. C. L. McCrory, A. Devadoss, X. Ottenwaelder, R. D. Lowe, T. D. P. Stack and C. E. D. Chidsey, *J. Am. Chem. Soc.*, 2011, **133**, 3696–3699.

19. V. L. N. Dias, E. N. Fernandes, L. M. S. da Silva, E. P. Marques, J. Zhang and A. L. B. Marques, *J. Power Sources*, 2005, **142**, 10–17.

20. Y. Lei and F. C. Anson, *Inorg. Chem.*, 1994, **33**, 5003–5009.

21. Q.-k. Zhuang and F. Scholz, *J. Porphyr. Phthalocyanines*, 2000, **4**, 202–208.

22. J. Zhang and F. C. Anson, *J. Electroanal. Chem.*, 1992, **341**, 323–341.

23. C. J. M. van der Ham, D. N. H. Zwagerman, L. Wu, J. P. Hofmann and D. G. H. Hetterscheid, *ChemElectroChem*, 2022, **9**, e202101365.

24. S.-J. Liu, C.-H. Huang and C.-C. Chang, *Mater. Chem. Phys.*, 2003, **82**, 551–556.

25. T. Gurusamy, P. Gayathri, S. Mandal and K. Ramanujam, *ChemElectroChem*, 2018, **5**, 1837–1847.

26. N. Tanjedrew, K. Thammanatpong, P. Surawatanawong, P. Chakthranont, T. Chantarojsiri, P. Sangtrirutnugul, K. Schwedtmann, K. Schwedtmann, J. J. Weigand and S. Kiatisevi, *ChemCatChem*, 2025, **17**, e01081.

27. C. X. Cai, K. H. Xue, X. Y. Xu and Q. H. Luo, *J. Appl. Electrochem.*, 1997, **27**, 793–798.

28. M. Wang, X. Xu, J. Gao, N. Jia and Y. Cheng, *Russ. J. Electrochem.*, 2006, **42**, 878–881.

29. N. C. Bhoumik, C. K. Locke, P. Mondol, Y. Yang and C. J. Barile, *ACS Appl. Energy Mater.*, 2025, **8**, 8130–8138.

30. S. N. Chowdhury, S. Biswas, P. Das, S. Paul and A. N. Biswas, *Inorg. Chem.*, 2020, **59**, 14012–14022.

31. L. Jin, S. Thanneeru, D. Cintron and J. He, *ChemCatChem*, 2020, **12**, 5932–5937.

32. N. W. G. Smits, B. van Dijk, I. de Bruin, S. L. T. Groeneveld, M. A. Siegler and D. G. H. Hetterscheid, *Inorg. Chem.*, 2020, **59**, 16398–16409.

33. X. Zhang, G.-S. Chen, H.-C. Liu, M.-J. Zhu, M.-Y. Xie, M.-S. Cen, Q.-J. Li, T.-S. Wang and H.-X. Zhang, *Electrochim. Acta*, 2023, **446**, 142099.

34. X. Zhang, X.-Q. Sun, J.-C. Liu, Y.-L. Pu, Q.-R. Ou-Yang, D.-Y. Lu and H.-X. Zhang, *Electrochim. Acta*, 2024, **477**, 143758.